Journal of Inorganic Biochemistry 186 (2018) 70–84

Contents lists available at ScienceDirect

Journal of Inorganic Biochemistry

journal homepage: www.elsevier.com/locate/jinorgbio

The *trans*-[Ru(PPh$_3$)$_2$(*N*,*N*-dimethyl-*N*′-thiophenylthioureato-k^{2}O,S)(bipy)] PF$_6$ complex has pro-apoptotic effects on triple negative breast cancer cells and presents low toxicity *in vivo*

Amanda Blanque Becceneri[a], Cecília Patrícia Popolin[a], Ana Maria Plutin[b], Edson Luis Maistro[c], Eduardo Ernesto Castellano[d], Alzir Azevedo Batista[e], Márcia Regina Cominetti[a,*]

[a] Departmento de Gerontologia, Universidade Federal de São Carlos, Rod. Washington Luís, Km 235, São Carlos, SP 13565-905, Brazil
[b] Facultad de Química, Universidad de la Habana, Zapata s/n entre G y Carlitos Aguirre, 10400 Habana, Cuba
[c] Departamento de Fonoaudiologia, Faculdade de Filosofia e Ciências, Universidade Estadual Paulista "Júlio de Mesquita Filho", Av. Hygino Muzzi Filho, 737, Marília, SP 17525-900, Brazil
[d] Instituto de Física de São Carlos, Universidade de São Paulo, CP 780, CEP 13560-970 São Carlos, SP, Brazil
[e] Departamento de Química, Universidade Federal de São Carlos, Rod. Washington Luís, Km 235, São Carlos, SP 13565-905, Brazil

ARTICLE INFO

Keywords:
Triple negative breast cancer
Ruthenium complexes
Acylthiourea ligands
In vivo studies
Apoptosis

ABSTRACT

Triple negative breast cancer (TNBC) is a heterogeneous subtype of breast tumors that does not exhibit the expression of estrogen and progesterone receptors, neither the amplification of the human epidermal growth factor receptor 2 (HER-2) gene. Despite all the advances in cancer treatments, the development of new anticancer drugs for TNBC tumors is still a challenge. There is an increasing interest in new agents to be used in cancer treatment. Ruthenium is a metal that has unique characteristics and important *in vivo* and *in vitro* results achieved for cancer treatment. Thus, in this work, with the aim to develop anticancer drugs, three new ruthenium complexes containing acylthiourea ligands have been synthesized and characterized: *trans*-[Ru(PPh$_3$)$_2$(*N*,*N*-dibutyl-*N*′-benzoylthioureato-k^{2}O,S)(2,2′-bipyridine (bipy))]PF$_6$ **(1)**, *trans*-[Ru(PPh$_3$)$_2$(*N*,*N*-dimethyl-*N*′-thiophenylthioureato-k^{2}O,S)(bipy)]PF$_6$ **(2)** and *trans*-[Ru(PPh$_3$)$_2$(*N*,*N*-dimethyl-*N*′-benzoylthioureato-k^{2}O,S)(bipy)]PF$_6$ **(3)**. Then, the cytotoxicity of these three new ruthenium complexes was investigated in TNBC MDA-MB-231 and in non-tumor MCF-10A cells. Complex **(2)** was the most selective complex and was chosen for further studies to verify its effects on cell morphology, adhesion, migration, invasion, induction of apoptosis and DNA damage *in vitro*, as well as its toxicity and capacity of causing DNA damage *in vivo*. Complex **(2)** inhibited proliferation, migration, invasion, adhesion, changed morphology and induced apoptosis, DNA damage and nuclear fragmentation of TNBC cells at lower concentrations compared to non-tumor MCF-10A cells, suggesting an effective action for this complex on tumor cells. Finally, complex **(2)** did not induce toxicity or caused DNA damage *in vivo* when low doses were administered to mice.

1. Introduction

Triple negative breast cancer (TNBC) is a heterogeneous subtype of breast cancer tumors that does not exhibit the expression of estrogen and progesterone receptors, neither the amplification of the human epidermal growth factor receptor 2 (HER-2) gene. TNBC is more aggressive to patients and has a worse prognosis when compared to other subtypes of the disease [1–3].

Despite of all the advances in cancer treatments the development of new anticancer drugs for TNBC tumors is still a challenge due to the lack of specific targets. Therefore, surgery, radiotherapy and systemic chemotherapy are the only available therapeutic options. Thus, it is pivotal to identify possible targets and to develop new treatments, which could be more specific for TNBC and have fewer side effects [1–3]. In this sense, and due to the previous success of the treatment with platinum-based drugs, such as cisplatin, there is increasing interest in new agents, especially metallodrugs, to be used in cancer treatment. Although cisplatin has presented good results in the treatment of some types of cancer, its use is limited by its severe adverse effects, such as cardiotoxicity, nephrotoxicity, ototoxicity and neurotoxicity [4–7].

Ruthenium is a metal that is receiving attention in the latest decades due to its unique characteristics and good results, *in vivo* and *in vitro*,

* Corresponding author.
E-mail address: mcominetti@ufscar.br (M.R. Cominetti).

https://doi.org/10.1016/j.jinorgbio.2018.05.011
Received 8 March 2018; Received in revised form 18 May 2018; Accepted 19 May 2018
Available online 24 May 2018

achieved for cancer treatment [8,9]. The most important properties of ruthenium complexes are the high rate of ligand exchange, an extensive range of accessible oxidation and the capacity to mimic iron in the biologic environment. These characteristics allow the development of a variety of complexes by the chemistry of coordination through the complexation of the metal with ligands that have already well known activities [10,11]. Thus, with the aim to develop novel anticancer drugs, three new ruthenium complexes, containing acylthiourea ligands have been synthesized and characterized. The compositions of the complexes are: *trans*-[Ru(PPh$_3$)$_2$(*N*,*N*-dibutyl-*N*′-benzoylthioureato-k^{2}O,S)(2,2′-bipyridine (bipy))]PF$_6$ **(1)**, *trans*-[Ru(PPh$_3$)$_2$(*N*,*N*-dimethyl-*N*′-thiophenylthioureato-k^{2}O,S)(bipy)]PF$_6$ **(2)** and *trans*-[Ru(PPh$_3$)$_2$(*N*,*N*-dimethyl-*N*′-benzoylthioureato-k^{2}O,S) (bipy)]PF$_6$ **(3)**. Subsequently, the cytotoxicity of these complexes against TNBC cells from the line MDA-MB-231 over MCF-10A non-tumor cells was investigated. The most selective was complex **(2)**, which was chosen for further studies to verify its effects on cell morphology, adhesion, migration, invasion, induction of apoptosis and DNA damage *in vitro*, as well as its toxicity and capacity of causing DNA damage *in vivo*.

2. Material and methods

All chemicals used to prepare the complexes are of analytical grade or of chemically pure grade. All the syntheses of the complexes were carried under argon atmosphere. The RuCl$_3$·3H$_2$O, KPF$_6$, triphenylphosphine (PPh$_3$), and 2,2′-bipy were used as received from Sigma-Aldrich. Detailed description of syntheses and characterization of related acylthioureas has been previously reported [12]. The identity of the products was confirmed by analysis of ^{1}H and ^{13}C NMR spectra in comparison to similar compounds previously reported in the literature [13–15].

2.1. Physical measurements

The spectrum in the infrared region (IR) was recorded on a FT-IR Bomem-Michelson 102 spectrometer in the 4000–250 cm^{-1} region, using cesium iodide (CsI) pellets. The ultraviolet–visible (UV–Vis) spectra of the complexes **(1–3)** in dichloromethane (CH_2Cl_2) were recorded on a spectrometer Hewlett Packard diode array-8452A. Molar conductivity values were obtained at 293 K using the complex in a solution at 10^{-3} mol·L^{-1} in CH_2Cl_2 and in a Meter Lab CDM2300 instrument. Nuclear magnetic resonance (NMR) was recorded on a Bruker DRX 400 MHz equipment, using tetramethylsilane as reference. Samples for ^{31}P{^{1}H} experiments were prepared under on inert atmosphere and measured at room temperature, with methylene chloride (CH_2Cl_2) as solvent and a D_2O capillary. Chemical shifts for phosphorus atoms were reported with respect to the phosphorus signal in 85% phosphoric acid (H_3PO_4), and $CDCl_3$ as used as a solvent for ^{1}H and ^{13}C NMR experiments.

Cyclic voltammetry (CV) experiments of the complexes, in solution, were conducted in an electrochemical analyzer BAS model 100B Instrument. These experiments were carried out at room temperature in CH_2Cl_2 containing 0.10 mol L^{-1} Bu_4NClO_4 (TBAP) (Fluka Purum) as a support electrolyte using a one-compartment cell, where the working and auxiliary electrodes were stationary Pt foils, and the reference electrode was Ag/AgCl, 0.10 mol L^{-1} TBAP in CH_2Cl_2. Under these conditions ferrocene was oxidized at 0.43 V (Fc^+/Fc). The microanalyses were performed in an EA 1108 CHNS microanalyser (Fisions Instruments).

2.2. Synthesis and characterization of the ruthenium complexes

The acylthiourea derivative (0.12 mmol) was dissolved in a Schlenk flask in 50 mL of a mixture of dichloromethane/methanol (2:1 v/v) with KPF$_6$ (0.12 mol; 15.0 mg). Next, 100 mg (0.11 mmol) of the *cis*-[RuCl$_2$(PPh$_3$)$_2$(bipy)] (*cis* chlorido). The solution was kept under reflux and stirring in an inert atmosphere for 24 hours (h). For each reaction, the final solution was concentrated to *ca.* 2 mL, and 10 mL of water was added to precipitate an orange powder. The solids were filtered off, washed with warm water (10 mL) and with diethyl ether (10 mL), and dried under vacuum.

Complex **(1)**: *trans*-[Ru(PPh$_3$)$_2$(*N*,*N*-dibutyl-*N*′-benzoylthioureato-k^{2}O,S)(bipy)]PF$_6$. ^{1}H NMR ppm: 8.89 and 8.15 (2H, C—H of bipy adjacent to the coordinated nitrogen atoms), 8.06–7.95 (m,5H atoms of Ph), 7.95–6.25 (30H atoms of PPh$_3$, and 6H aromatic of bipy); 4.88 (d; *J* = 7.08 Hz; 2H, CH_2); 3.47–3.82 (8H; q; CH_2); 2.07–1.70 (2H; m; CH2); 0.93–0.98 (t; 6H, CH3; *J* = 7.01 Hz). ^{13}C NMR, ppm: 174.06 (CS); 170.26 (CO); 156.99, 155.80, 154.96, 151.41, 149.22, 138.76, 138.61, 136.66, 136.54, 133.31, 133.11, 133.00, 132.90, 132.31, 131.87, 131.48, 130.05, 128.97, 128.78, 128.71, 128.19, 128.10, 127.97, 127.79, 126.12, 123.57, 123.19 (C-Ph; C-bipy, C-PPh3); 51.46 (CH_2); 50.64 (CH_2); 19.66 (CH_2); 13.66 (CH_3); ^{31}P {^{1}H} ppm: 27.69 (s); IR (cm^{-1}): (νCHPPh$_3$, bipy, Th) 3080, 3059, 3028, 2922, 2853; (νC=N$_{bipy}$)1603; (νC=O) 1585; (νC=N and νC=C) 1508, 1495, 1481, 1470, 1450, 1433, 1412, 1400, 1354; (νCS) 1267; (δCH2) 1207; (νC—P) 1088; (ν_{ring}) 1072, 1028, 1001; (νP—F) 839; (νC—S) 758; (νRu—P) 521; (νRu—S) 490; (νRu—N) 405; (νRu—O) 360. Λ_m = 57.6 Ω^{-1} cm^2 mol^{-1}. UV–Vis (CH_2Cl_2, 10^{-5} M): λ/nm (ε/mol^{-1} L cm^{-1}) 286 (4770), 403 (873), 472 (652). Elemental analyses for $C_{62}H_{61}F_6N_4OP_3RuS$: calcd. (exp)%, C, 61.13 (61.31); H, 5.04 (5.19); N, 4.60 (4.44); S, 2.63 (2.78).

Complex **(2)**: *trans*-[Ru(PPh$_3$)$_2$(*N*,*N*-dimethyl-*N*′-thiophenylthioureato-k^{2}O,S)(bipy)]PF$_6$. ^{1}H NMR ppm: 8.98–8.14 (2H, C—H of bipy adjacent to the coordinated nitrogen atoms), 7.84–6.73 (30H atoms of PPh$_3$, and 6H aromatic of bipy, 3H aromatic of thiophene), 2.90 (3H, s, CH_3), 2.80 (3H, s, CH_3). ^{13}C NMR ppm: 173.16 (CS); 169.19 (CO); 157.90, 156, 80, 155.90, 154.85, 151. 22, 150.07, 149. 07, 140.29, 138.69, 138.29, 137.49, 136,64, 136.50, 134.09, 133.81, 133.28, 133.05, 132.40, 130.84, 130.25, 129.30, 128.21, 127.88, 127.66, 127.45, 127.25, 16, 124.93, 123.52, 122.53 (C-Ph; C-bipy, C-PPh$_3$); 24.63(CH_3); 18.55 (CH_3); ^{31}P{1H} NMR ppm: 27.75 (s); IR (cm^{-1}): (νCHPPh$_3$, bipy, Th) 3080, 3059, 2922, 2852; (νC=N bipy) 1603; (νC=O) 1578; (νC=C thiophenyl) 1512; (νC=N and νC=C) 1491,1481, 1471, 1456, 1435, 1418, 1391, 1358; (νCS) 1292; (νC—P) 1090; (ν_{ring}) 1072, 1026,; (νP—F) 841; (νC—S) 766; (νRu—P) 520; (νRu—S) 496; (νRu—N) 403; (νRu—O) 357. Λ_m = 58.9 Ω^{-1} cm^2 mol^{-1}. UV–Vis (CH_2Cl_2, 10^{-5} M): λ/nm (ε/mol^{-1} L cm^{-1}) 278 (4720), 405 (900), 472 (644). Elemental analyses for $C_{54}H_{47}F_6N_4OP_3RuS_2$, calcd.(exp)%, C, 56.89 (56.75); H, 4.15 (4.26); N, 4.91 (5.11); S, 5.63 (5.71).

Complex **(3)**: *trans*-[Ru(PPh$_3$)$_2$(*N*,*N*-dimethyl-*N*′-benzoylthioureato-k^{2}O,S) (bipy)]PF$_6$·^{1}H NMR ppm: 9.21 and 8.22 (2H, C—H of bipy adjacent to the coordinated nitrogen atoms), 7.86–7.81 (m; 5H; Ph); 7.88–6.95 (m, 30H atoms of PPh$_3$, and 6H aromatic of bipy), 3.58 (3H; s; CH_3) and 3.20 (3H; s; CH_3). ^{13}C NMR ppm: 174.06 (CS); 170.26 (CO); 156.99, 155.80, 154.96,151.41, 149.22,138.76, 138.61, 136.66, 136.54, 133.31, 133.11, 133.00, 132.90, 132.31, 131.87, 131.48, 130.05, 128.97, 128.78, 128.71, 128.19, 128.10, 127.97, 127.79, 126.12, 123.57, 123.19 (C-Ph; C-bipy, C-PPh$_3$), (CH_3); 41.69 (CH_3); 40.50 (CH3); ^{31}P{^{1}H} NMR ppm: 21.76 (s). IR (cm^{-1}): (νCHPPh$_3$, bipy, Th) 3078, 3055, 2922, 2853; (νC=N bipy) 1603; (νC=O) 1588; (νC=C and νC=N)1500, 1489, 1489, 1479, 1435, 1402, 1356; (νC—S)1294; (ν—P) 1090; (ν_{ring}) 1072, 1024, 1001; (νP—F) 841; (νC—S) 764; (νRu—P) 517, (νRu—S) 492; (νRu—N) 403; (νRu—O) 355. Λ_m = 52.8 Ω^{-1} cm^2 mol^{-1}. UV–Vis (CH_2Cl_2, 10^{-5} M): λ/nm (ε/mol^{-1} L cm^{-1}) 282 (4730), 407 (900), 476 (654). Elemental analyses for $C_{56}H_{49}F_6N_4OP_3RuS$, calcd.(exp)%, C, 59.31 (59.48); H, 4.35 (4.27); N, 4.94 (4.79); S, 2.83 (2.74).

2.3. Crystal structure determination

Single crystals suitable for X-ray diffraction were obtained by slow evaporation of $CHCl_3$: *n*-hexane (3:1) solutions of the complex **(3)**. Diffraction data were collected on an Enraf-Nonius Kappa CCD

diffractometer with graphite-monochromated Mo Ka radiation (λ = 0.71073 Å). The final unit cell parameters were based on all reflections. Data collections were performed using the COLLECT program [16]; integration and scaling of the reflections were performed with the HKL Denzo-Scalepack system of programs [17]. Absorption corrections were carried out using the Gaussian method [18]. The structures were solved by direct methods with SHELXS-97. The models were refined by full-matrix least-squares on F2 by means of SHELXL-97 [19]. The projection views of the structures were prepared using ORTEP-3 for Windows [20]. Hydrogen atoms were stereochemically positioned and refined with the riding model.

2.4. In vitro assays

2.4.1. Cell lines

MDA-MB-231 cells were obtained from Rio de Janeiro Cell Bank, maintained at 37 °C in 5% CO_2 in Dulbecco's Modified Eagle Medium (DMEM, Vitrocell), containing Fetal Bovine Serum (FBS) 10%, L-glutamine (2 mM), penicillin (100 UI/mL) and streptomycin (100 mg/mL). The non-tumor breast cell line MCF-10A was obtained from Peter MacCallum Cancer Centre, Australia, maintained at 37 °C in 5% CO_2 in Dulbecco's Modified Eagle Medium and Nutrient Mixture F-12 (DMEM/F12, Life Technologies) supplemented with 5% horse serum, EGF (0.02 mg/mL), hydrocortisone (0.05 mg/mL), insulin (0.01 mg/mL), L-glutamine (2 mM), penicillin (100 UI/mL) and streptomycin (100 mg/mL).

2.4.2. Complexes

The complexes for the *in vitro* assays were solubilized in Dimethyl Sulfoxide (DMSO, 100%) and then the concentrations were prepared using the appropriate culture medium. The final concentration of DMSO was 0.1% in each sample.

2.4.3. Cell cytotoxicity assay

The effect of the complexes **(1–3)** on cytotoxicity of MDA-MB-231 and MCF-10A cells was determined using MTT [3-(4,5-dimethylthiozol-2-yl)-2,5-diphenyltetrazolium bromide] according to Mosmann [21], with modifications. MDA-MB-231 and MCF-10A cells (1×10^4/100 μL) were seeded in appropriate medium in sterile 96-well plates. Cells were maintained at 37 °C and 5% CO_2 for 24 h in a cell culture incubator. After, the cells were incubated or not (control) with different concentrations of the complexes **(1–3)** (0, 0.39, 0.78, 1.56, 3.12, 6.25, 12.5, 25 or 50 μM). Then, the cells were incubated for additional 24 h under the same conditions described above. After incubation, a solution containing MTT (1 mg/mL) was added to the wells (100 μL/well). The plates were then kept for 4 h at 37 °C and the crystals formed were diluted in DMSO (100%). The absorbance was read on an ELISA plate reader (Labtech LT4000) at wavelength of 540 nm. In the control, the cells were incubated with appropriate culture medium and with the vehicle used to solubilize the complexes, DMSO (0.1% final concentration). The selectivity index (SI) was calculated as the ratio: the half-maximal inhibitory concentration 50% (IC_{50}) (MCF-10A)/IC_{50} (MDA-MB-231).

2.4.4. Cell morphology

Cell morphology was determined as describer earlier [22]. Briefly, MDA-MB-231 and MCF-10A cells were seeded (1×10^5/1000 μL) in appropriate medium into sterile 12-wells plates. Cells were allowed to grow at 37 °C in 5% CO_2 for 24 h in a cell culture incubator and then, treated or not (control) with 12.5 μM of the complex **(2)** for 2 and 24 h. Cells were viewed using an inverted microscope (Nikon Eclipse TS100) with amplification of 40× and images were captured with a camera (Moticam 1000 - 1.3 MP Live Resolution).

2.4.5. Colony formation

MDA-MB-231 cells were seeded (3×10^2/2000 μL) in appropriate medium into sterile 6 cm Petri dishes and incubated at 37 °C and 5% CO_2 for 24 h in a cell culture incubator. Following the time, the cells were incubated or not (control) with different concentrations of the complex **(2)** (0.5, 1 or 2 μM) for 2 h. After the period, the medium was removed, the cells gently washed with phosphate buffered saline (PBS) and appropriate culture medium was added. The cells were again incubated at 37 °C and 5% CO_2 for 10 days. After incubation, the supernatant was discarded and cells were fixed with a solution of methanol and acetic acid (3:1) for 5 minutes (min) and stained with a solution of methanol and crystal violet at 5% for 15 min, as describer earlier [23]. The plates were photographed and then the colonies were counted, and their size was measured using Image J software.

2.4.6. Migration assay

Transwell assays in Boyden chambers and wound healing assays, as already described [23], were used to analyze the effects of the complex **(2)** on migration of MDA-MB-231 and MCF-10A cells. For the assay using Boyden chambers, MDA-MB-231 and MCF-10A cells were seeded (5×10^4/350 μL) in appropriate incomplete medium (without FBS), incubated or not (control) with different concentrations (1, 2 or 4 μM) of the complex **(2)** in the upper chamber of migration inserts. Supplemented medium with serum (10%) was added to the lower chamber to act as a chemoattractant of the migration, except for the negative control, which did not receive serum in the lower chamber. Cells were maintained in a humid incubator with 5% CO_2 at 37 °C for 22 h. Then, the remaining cells in the upper chamber were removed using a cotton swab. After, cells that were able to migrate to the other side of the insert membrane were fixed with methanol for 5 min and stained with 1% of toluidine blue solution. The membranes of each insert were removed, prepared on slides and integrally counted with the help of a microscope (Coleman N-120). Representative images of each membrane were taken with a camera (Moticam 1000 - 1.3 MP Live Resolution) at 40× magnification.

For the wound healing assay, MDA-MB-231 and MCF-10A cells (1×10^5/1000 μL) were plated into sterile 12-wells plates and incubated in a humid incubator with 5% CO_2 at 37 °C until the culture reached 100% of confluence. Subsequently, a scratch was made with a sterile pipette tip and cells were washed with PBS to remove detached cells. Cells were incubated with complex **(2)** (1 μM) for 24 h. The images were taken with a camera (Moticam 1000 - 1.3 MP Live Resolution) at 40× magnification at 0 and 24 h.

2.4.7. Invasion assay

The effects of complex **(2)** on cell invasion were determined by the capacity of the cells to transmigrate through a layer of matrigel in a transwell chamber (Corning) with 8 μm pores according to Fuzer et al. [24]. Briefly, the inserts were previously hydrated with serum free medium for 2 h in a humid environment at 37 °C. MDA-MB-231 and MCF-10A cells (5×10^4/350 μL) were seeded in the upper chamber of the inserts in serum free medium, treated or not (control) with different concentrations (1, 2 or 4 μM) of the complex **(2)**. Supplemented medium with serum (10%) was added to the lower chamber to act as chemoattractant of the invasion, except for the negative control, which did not receive serum in the lower chamber. The plate was maintained in a humid incubator with 5% CO_2 at 37 °C for 22 h. Then, the cells remaining in the upper chamber were removed using a cotton swab. Cells that were able to invade through the matrigel layer reaching the other side of the insert membrane were fixed with methanol for 5 min and stained with 1% of toluidine blue solution. The membranes of each insert were removed, prepared on slides and integrally counted with the help of a microscope (Coleman N-120). Representative images of each membrane were taken with a camera (Moticam 1000 - 1.3 MP Live Resolution) at 40× magnification.

2.4.8. Adhesion assay

The effects of complex **(2)** on the adhesion of MDA-MB-231 cells

were analyzed in 96 well plates, as described earlier [24]. Briefly, vitronectin (1 μg), laminin (0.3 μg) or fibronectin (0.3 μg) were immobilized on the plates in a cell adhesion buffer (20 mM HEPES, 150 mM NaCl, 5 mM KCl, 1 mM $MgSO_4$ and 1 mM $MnCl_2$ pH 7.35) overnight at 4 °C. For collagen type I, plates ready with collagen type I (10 μg) precoated were used (BD Biosciences). After, the plates were blocked with adhesion buffer (20 mM HEPES, 150 mM NaCl, 5 mM KCl, 1 mM $MgSO_4$ and 1 mM $MnCl_2$ pH 7.35) containing 1% bovine serum albumin (BSA) for 1 h and then the wells were washed with 100 μL of adhesion buffer. MDA-MB-231 cells (5×10^4/300 μL) was harvested, counted and incubated for 30 min treated or not (control) with different concentrations of the complex **(2)** (2, 4 or 8 μM) at 37 °C and 5% CO_2 in a cell culture incubator and then seeded and incubated under the same conditions for a further 1 h. Subsequently, the non-adherent cells were carefully removed by PBS washing and the adhered cells were fixed with 100 μL of 70% ethanol for 10 min and stained with 0.5% violet crystal for 20 min. Excess dye was removed by washing the wells with PBS. The stained cells were diluted in 1% sodium dodecyl sulfate solution (SDS) for 30 min. The absorbance was read on ELISA plate reader (Labtech LT4000) at wavelength of 540 nm.

2.4.9. Phalloidin staining

The effects of complex **(2)** on the F-actin cytoskeleton was verified with Alexa Fluor® 488 Phalloidin (Life Technologies) as described earlier [22]. MDA-MB-231 cells (5×10^4 cells/100 μL) were plated into sterile black 96-well plates and maintained at 37 °C in a humidified incubator with 5% CO_2 for 24 h. After, the cells were treated or not (control) with different concentrations (2, 4, 8 or 16 μM) of the complex **(2)** and incubated for 2 h. Next, the cells were washed with PBS, fixed with 4% paraformaldehyde in PBS for 30 min and then permeabilized with 0.1% Triton-X 100 in PBS for 5 min at room temperature. Then, the plates were blocked with 2% BSA for 30 min, followed by the addition of Alexa Fluor® 488 Phalloidin for 20 min. After, the cells were stained with 4′,6-diamidino-2-phenylindole (DAPI) (Life Technologies) for 4 min and washed gently three times with fresh PBS. Images were obtained with the help of an automated microscope ImageXpress® Micro XLS System (Molecular Devices) with amplification of 40×.

2.4.10. Apoptosis assay by flow cytometry

The apoptotic activity of complex **(2)** on MDA-MB-231 and MCF-10A cells was analyzed by flow cytometry using the Phycoerythrin-Annexin V (PE-Annexin-V) Apoptosis Detection Kit (BD Biosciences), as already described [22]. In short, MDA-MB-231 and MCF-10A cells were seeded (5×10^4/1000 μL) in appropriate culture medium into sterile 24-wells plates. The cells were allowed to grow at 37 °C in 5% CO_2 for 24 h in a cell culture incubator and after, treated or not (control) with different concentrations (2, 4 or 8 μM) of the complex **(2)** for 2 h. Later, the plate was centrifuged at 2000 rpm for 5 min at 4 °C, the cells were washed with PBS and resuspended in 200 μL of binding buffer provided by the kit. Then, the cells were incubated with 5 μL of 7-Aminoactinomycin D (7AAD) and 5 μL PE-Annexin-V for 15 min. After the incubation time the supernatant was removed and 300 μL binding buffer was added to the wells. The cells were then removed from the wells with a scraper and transferred to cytometry tubes. Cells were analyzed through 20,000 events in Accuri C6 flow cytometer (BD Biosciences) and the fluorescence was quantified by CSampler software (BD Biosciences). As a positive control of apoptosis, camptothecin (32 μM), an apoptosis-inducing chemotherapeutic agent was used [25].

2.4.11. DAPI staining

To verify if complex **(2)** induces nuclear fragmentation, a process that occurs during cell apoptosis, DAPI staining was performed, as described earlier [22]. MDA-MB-231 and MCF-10A cells were seeded (1×10^4/100 μL) in appropriate culture medium into sterile black 96-wells plates and incubated at 37 °C and 5% CO_2 for 24 h in a cell culture incubator. After incubation, cells were treated or not (control) with different concentrations (2, 4 and 8 μM) of the complex **(2)** for 2 h. Then, cells were washed with PBS and then fixed with methanol for 10 min. Once fixed, the cells were stained with 1 μg/mL DAPI (Life Technologies) diluted in PBS for 10 min. Next, the cells were washed 3 times with PBS. Fluorescence was captured in automated microscope ImageXpress® Micro XLS System (Molecular Devices) with amplification of 40×. As a positive control of apoptosis, staurosporine (0.5 μM), which is recognized for inducing apoptosis in different cell lines [26], was used.

2.4.12. Cell cycle

To verify whether the complex **(2)** is able to arrest cell cycle, propidium iodide (PI) staining was performed, as described earlier [27]. MDA-MB-231 and MCF-10A cells were seeded (5×10^5/1000 μL) in appropriate culture medium into 6 cm Petri dishes and maintained at 37 °C in a humidified incubator with 5% CO_2 for 24 h. After, cells were treated or not (control) with different concentrations of the complex **(2)** (0.5, 1 and 2 μM) for 24 h and maintained under the same conditions described above. Next, the cells were harvested, centrifuged and washed with cold PBS. Then, the cells were fixed in 70% cold ethanol and stored for 24 h at −20 °C. After the period, cells in PBS were incubated with Ribonuclease (RNase) A (0.02 mg/mL) (Sigma-Aldrich) at 37 °C for 30 min. After the incubation, cells were stained with a binding buffer containing PI (10 μg/mL) (Sigma-Aldrich). Finally, the DNA content was determined by flow cytometry in Accuri C6 flow cytometer (BD Biosciences) through 20,000 events using CSampler software (BD Biosciences). As positive control, camptothecin (32 μM) was used.

2.4.13. Real time quantitative PCR (qRT-PCR) assay

Expression of apoptosis-related genes was verified by real-time quantitative PCR as described earlier [22]. For this, MDA-MB-231 and MCF-10A cells were seeded (1×10^6/2000 μL) in appropriate medium into sterile 6 cm Petri dishes and incubated at 37 °C and 5% CO_2 for 24 h in a cell culture incubator. Following the time, cells were treated or not (control) with different concentrations (4, 8 or 16 μM) of the complex **(2)** for 2 h. Total RNA was extracted using Trizol reagent (Invitrogen). cDNAs were synthesized using Enhanced Avian RT First Strand Synthesis Kit (Sigma-Aldrich). A CFX96 Touch Real-Time PCR Detection System Analyzer (Bio-Rad) was used to amplify both target and internal control templates (1 cycle at 95 °C for 5 min and 40 amplification cycles at 95 °C for 30 s, 55 °C for 30 s and 72 °C for 45 s). In brief, 1 μL of reverse transcribed product template, 5 μL of SYBR Green JumpStart Taq ReadyMix (Sigma-Aldrich) and the gene-specific primer pairs at a final concentration of 500 nmol L^{-1} for each primer, made 10 μL of reaction system. Primers used in the assays were: Caspase-3 (Forward: 5′GTG CTA CAA TGC CCC TGG AT3′; Reverse: 5′CAT TCA TTT ATT GCT TTC C3′), Bax (Forward: 5′CAT CCA GGA TCG AGC AGG3′; Reverse: 5′CGA TGC GCT TGA GAC ACT C3), Bcl-2 (Forward: 5′GGT GGG AGG GAG GAA GAA T3′; Reverse: 5′GAG GCA TCA CAT CGA C3′) and β-actin (Forward: 5′GAC GGC CAG GTC ATC ACC ATT G3′; Reverse: 5′AGC ACT GTG TTG GCG TAC AGG 3′). Bax primers (NM_001291428.1) and Bcl-2 (NM_000633.2) were designed with Gene Runner (version5.0.63 Beta), except for the primer Caspase-3 (NM_004346.3). For each gene, all samples were amplified simultaneously in triplicate in one assay run. The internal calibrator used as a basis to standardize the results of expression was the control group ΔCts average. Calibration was determined by ΔΔCt = ΔCt (sample) − ΔCt (calibrator). Gene expression was assessed by relative quantification, using the formula $2-\Delta\Delta Ct$ [28] and β-actin as internal control. A blank with water, primers and SYBR Green instead of sample was performed.

2.4.14. SDS-PAGE and Western blotting

MDA-MB-231 cells were seeded (1×10^6/2000 μL) in appropriate medium into sterile 6 cm Petri dishes and incubated at 37 °C and 5% CO_2 for 24 h in a cell culture incubator. Following the time, cells were treated or not (control) with different concentrations (0.5, 1, 2, 4, 8 or

16 μM) of the complex **(2)** for 4 h. After incubation, cells were lysed using CelLytic™ M buffer (Sigma-Aldrich). Protein concentrations of supernatants were determined using BCA Protein Assay Kit (Thermo Scientific). Protein samples (15 μg) were applied onto a 4–20% PAGE Mini-PROTEAN TGX™ Precast gels (BioRad), transferred to nitrocellulose membranes (BioRad) and incubated with anti-Caspase-3, anti-Bax and anti-Bcl-2 antibodies (ABCAM) (1:1000), followed by incubation with HRP-conjugated anti-mouse secondary antibody (1:5000) (ABCAM). Beta-actin was used as endogenous control. Substrate development was performed using Clarity™ Western ECL substrate (BioRad). Specific bands were visualized with ChemiDoc MP imager (BioRad).

2.4.15. Comet assay

The comet assay was performed according to Tice et al. [29] with modifications. Briefly, MDA-MB-231 and MCF-10A cells were seeded (1×10^5/1000 μL) into sterile 12-wells plates. Cells were allowed to grow at 37 °C in 5% CO_2 for 24 h and then treated or not (control) with different concentrations (2, 4 or 8 μM) of the complex **(2)** or positive control cisplatin (8 μM) for 1 h. After this period, the cells were harvested, centrifuged and resuspended in 500 μL of culture medium. Then, 20 μL of this cell suspension were mixed with 120 μL of 0.5% low-melting point agarose and dropped on slides precoated with 1.5% normal melting point agarose and taken to a cold lysis solution (NaCl 2.5 M, Ethylenediamine Tetraacetic Acid (EDTA)-titriplex 100 mM, Tris 10 mM, Triton X-100 1%, DMSO 10% (pH 10)) for 1 h. After denaturation (20 min) and alkaline electrophoresis (25 V, 300 mA, 20 min) the slides were neutralized (0.4 M Tris-HCl, pH 7.5) for 15 min and fixed (ethanol 100%). The staining of the slides was performed with GelRed (Uniscience) and comet blind analysis of at least 150 randomly cells per group was done visually [30], according to tail size using a fluorescence microscope (Olympus BX61-TRF5). These cells were scored into the following four classes: class 0, no tail; class 1, tail shorter than the diameter of the head (nucleus); class 2, tail length one

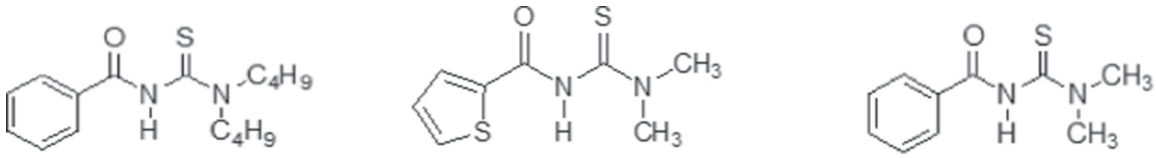

(1) **(2)** **(3)**

Fig. 1. Representative structures of the ligands. (1) *N*,*N*-dibutyl-*N*′-benzoylthiourea; (2) *N*,*N*-dimethyl-*N*′-thiophenylthiourea; (3) *N*,*N*-dimethyl-*N*′-benzoylthiourea.

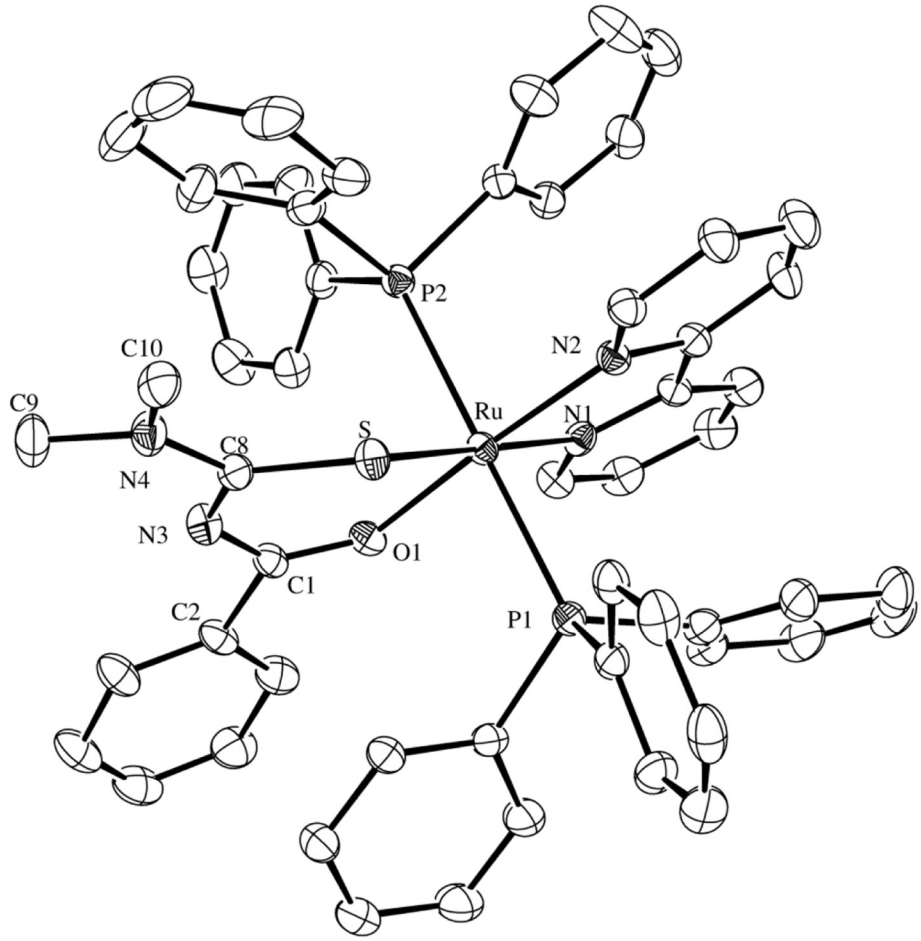

Fig. 2. ORTEP view of complex **(3)** showing 50% probability ellipsoids. Hydrogen atoms, the PF_6^- anion and some labels of the ligands are omitted for clarity.

Table 1
IC_{50} (μM) for complexes **(1–3)** in MDA-MB-231 and MCF-10A cells after 24 h of incubation. SEM = standard error of the mean.

Complex	IC_{50} (μM) ± SEM		[a]SI
	MDA-MB-231	MCF-10A	
(1)	21.92 ± 0.05	7.92 ± 2.09	0.36
(2)	8.81 ± 0.81	14.82 ± 2.50	1.67
(3)	9.33 ± 0.62	8.82 ± 0.66	0.94
Cisplatin[b]	2.43 ± 0.20	29.45 ± 0.85	12.06
bipy	>100	>100	–
PPh_3	>100	>100	–
Acylthioureas	>100	>100	–

[a] SI = selectivity index of the complexes.
[b] The cisplatin was dissolved in dimethylformamide [22].

to two times the diameter of the head; and class 3, tail length more than twice the diameter of the head. Cells with all the DNA in the tail, class 4, were disregarded due to the high probability that they are already dead [31]. The score was calculated by the sum of the multiplication of the number of cells in each class by the damage class.

2.5. In vivo assays

2.5.1. Animals

The toxicity and comet assays were carried out in male Swiss mice (*Mus musculus*) at an age of 10–12 weeks weighing approximately 20–25 g. Mice were kept in a climate-controlled environment (22 ± 2 °C) with cycles of 12 h light/dark cycle and with *ad libitum* access to food and water. The animal procedures were approved by the Ethics Committee of UFSCar (CEUA n°1051160315) and UNESP (CEUA/FAMEMA n°828/2016).

2.5.2. Acute toxicity

The acute toxicity assay was conducted in accordance to the Organisation for Economic Cooperation and Development (OECD), Acute Toxic Class Method – Guide 423 [32], with modifications. In our assay, doses were administrated intraperitoneally and not orally. Doses of 50 and 300 mg/kg of the complex **(2)** were administrated, following the order established by the guide, in two groups of three animals, totaling six animals in each treatment group. The negative control group received only the vehicle (saline solution and DMSO). Then, the animals were observed individually for the first 30, 60, 120, 180 and 240 min after administration of complex **(2)** and subsequently once a

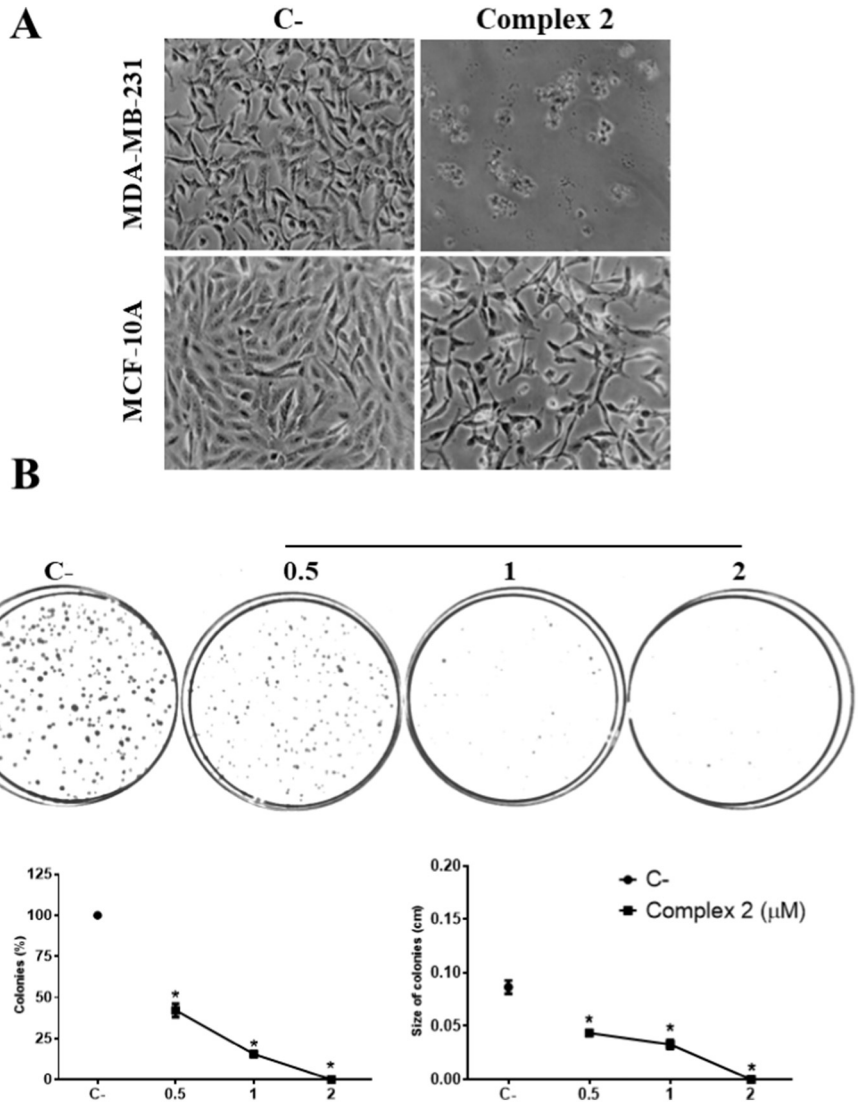

Fig. 3. Cytotoxicity effects of complex **(2)** on MDA-MB-231 and MCF-10A cells. (A) Cell morphology was examined 24 h of treatment at 12.5 μM of the complex **(2)**. (B) Clonogenic assay of MDA-MB-231 cells treated or not (control) with different concentrations (0.5, 1 or 2 μM) of complex **(2)** for 2 h. The experiments were performed in triplicate. Images correspond to one of triplicates. Results were compared with negative control (C−) (untreated) (*$p \leq 0.01$).

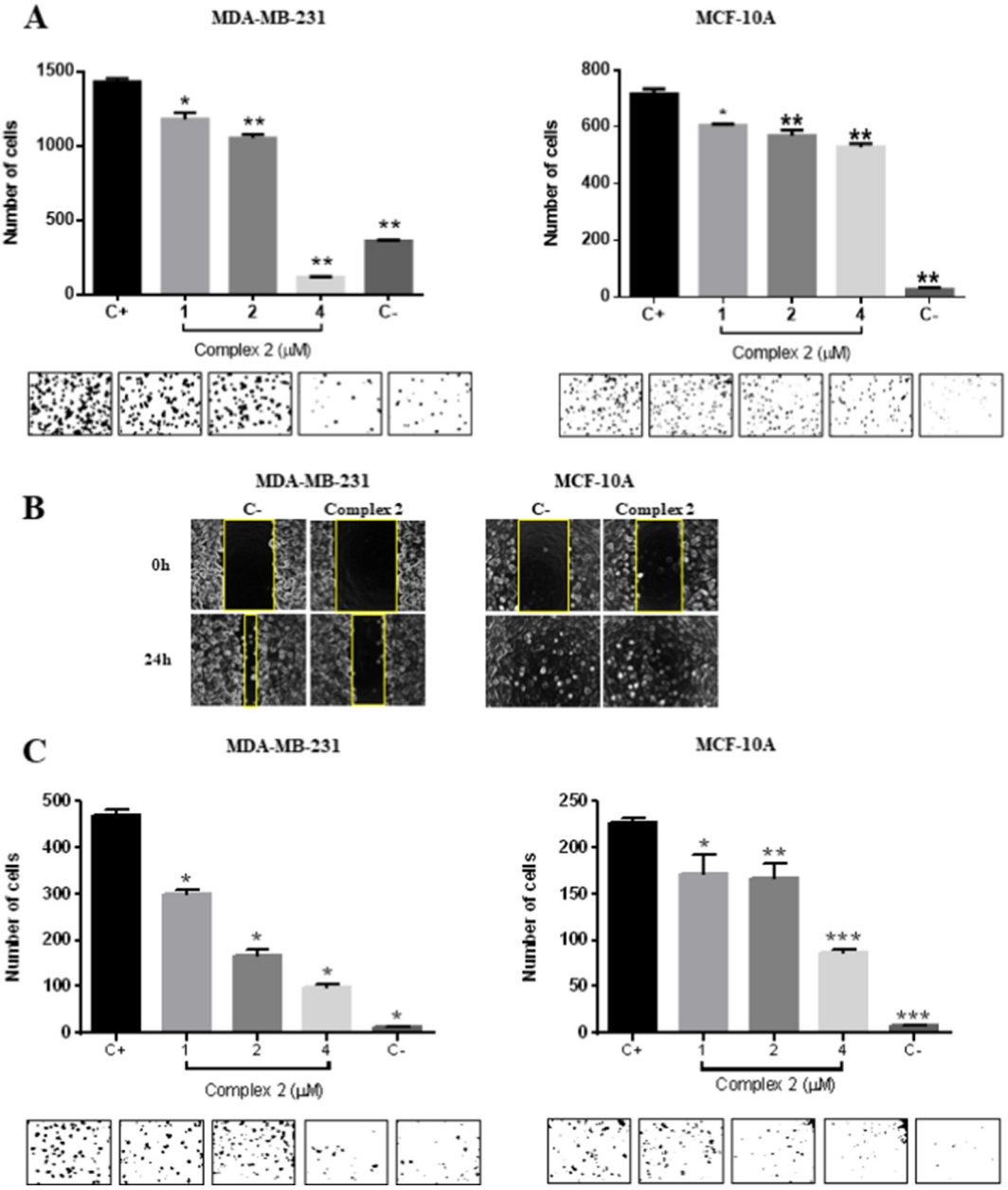

Fig. 4. Effects of complex **(2)** on cellular migration and invasion of MDA-MB-231 and MCF-10A cells. (A) Boyden chambers migration assay at 22 h of treatment with 1, 2 or 4 μM of the complex **(2)**. Positive control (C+) represents cells without any treatment and negative control (C−) was cells toward an FBS-free medium. (B) Wound healing assay at 0 and 24 h of treatment with 1 μM of the complex **(2)**. Results were compared with control (C−). (C) Cell invasion thorough matrigel at 22 h of treatment with 1, 2 or 4 μM of the complex **(2)**. Positive control (C+) represents cells without any treatment and negative control (C−) was cells toward an FBS-free medium. The experiments were performed in triplicate. Images correspond to one of triplicates. (*$p \leq 0.05$, **$p \leq 0.01$, ***$p \leq 0.001$).

day for 14 days to identify possible symptoms related to toxicity and/or deaths. The animals also were weighed five times during the experiment. At the end of the experiment, the animals were euthanized, and organs related to metabolism (heart, spleen, liver and kidneys) were weighed and visually analyzed.

2.5.3. Histological analysis

The collected organs (heart, liver, kidney and spleen) were fixed in 10% buffered formalin for 24 h and washed in running water for 1 h. Then, the organs were submitted to a histological procedure in which they underwent dehydration stages, clarification and impregnation. After, the organs were paraffin embedded and then the paraffin blocks obtained were cut longitudinally, in relation to the organ, by means of a rotating microtome (Leica), obtaining semi-serial cuts with thickness of 5 μm. Next, the staining process was performed with hematoxylin and eosin (HE) for morphological and structural analysis. The slides were scanned in the panoramic desk (3DHISTECH) and the photos analyzed with the 3DHISTECH software.

2.5.4. In vivo comet assay

The *in vivo* comet assay was performed based on the *In Vivo Mammalian Alkaline Comet Assay*, Guide TG 489 of the OECD [33]. Mice were divided into five groups with five animals in each. The complex **(2)** (12.5, 25 or 50 mg/kg), positive control doxorubicin (20 mg/kg) or negative control (treated only with the vehicle - saline solution and DMSO) were administered intraperitoneally for 3 days at 24 h interval. On the third day, peripheral blood (20 μL) were collected 4 h after the administration of the last treatment to avoid DNA repair. Then, the

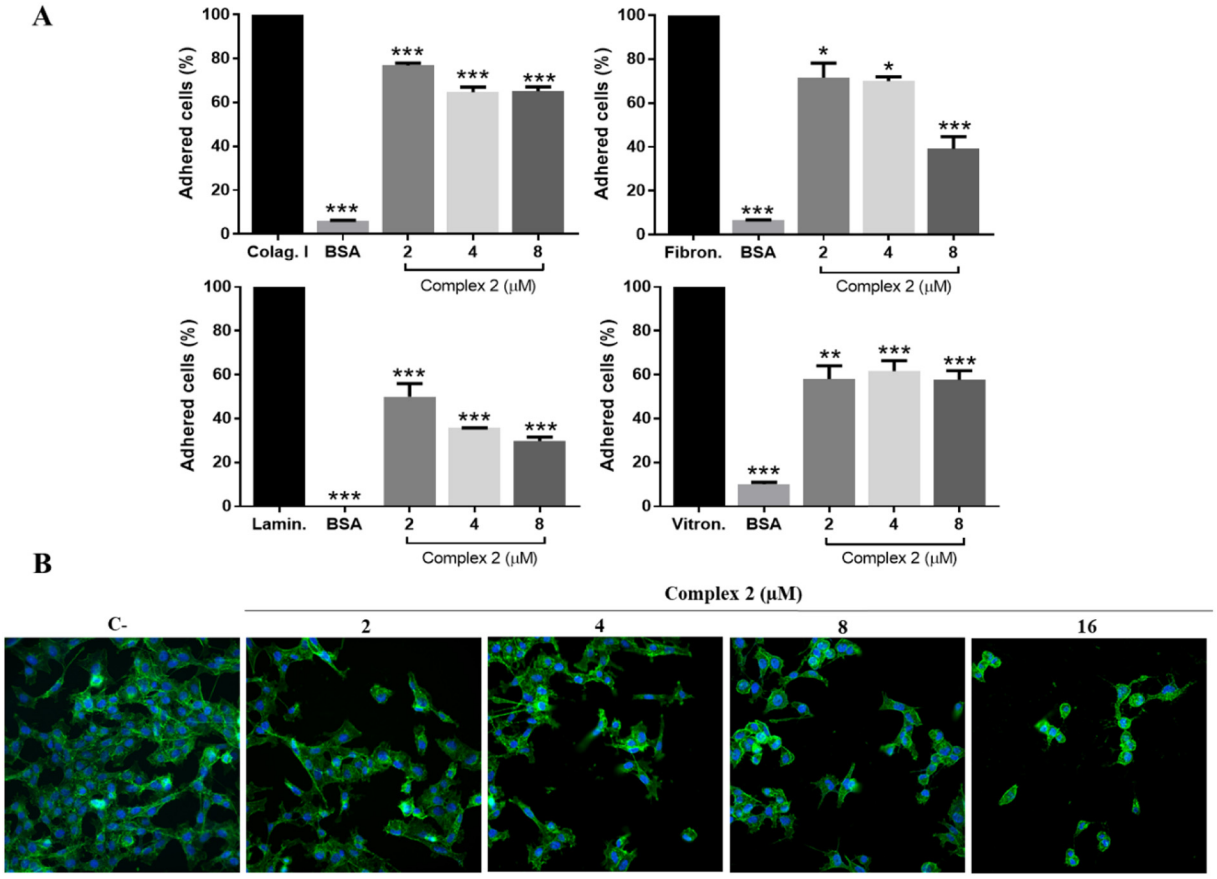

Fig. 5. Effects of complex **(2)** on cell adhesion and cytoskeleton of MDA-MB-231 cells. (A) Cell adhesion assay with type I collagen, fibronectin, laminin and vitronectin after 1 h and 30 min of treatment with 2, 4 or 8 μM of the complex **(2)**. (B) Cytoskeleton assay with phalloidin and DAPI after 2 h of treatment with 2, 4, 8 or 16 μM of the complex **(2)**. The experiments were performed in triplicate. Images correspond to one of triplicates. Results were compared with control (C−) (untreated) (*$p \leq 0.05$, **$p \leq 0.01$, ***$p \leq 0.001$).

same steps of the *in vitro* comet assay were performed.

2.5.5. Statistical analysis

Each experiment was repeated three times in triplicate and a standard error (SE) mean was calculated. Shapiro-Wilk's test was used to verify data normality. As normal distribution was present, the results were compared statistically with a one-way or two-way analysis of variance (ANOVA). Since the ANOVA tests showed significant differences (acceptable p level < 0.05), Turkey's significant difference *post hoc* analyses were performed to determine differences between simple and grouped main-effect means, respectively. The data were analyzed and IC_{50} calculations were made using Hill's equation in the GraphPad Prism software (version 6.05).

3. Results and discussion

3.1. Synthesis, characterization and crystal structure determination

Given the promising results of ruthenium as potential anti-tumor drug, three complexes were synthesized and characterized. Subsequently, their effects on TNBC cells from the line MDA-MB-231 over MCF-10A non-tumor cell were investigated. The complexes were synthesized according to the general method previously reported [34]. The one-pot procedure involves the reactions between the precursor *cis*-$[RuCl_2(PPh_3)_2(bipy)]$ complex with *N*-Acyl-*N*′, *N*′-disubstituted thiourea derivatives (Fig. 1), producing complexes with good yield, with the general formula *trans*-$[Ru(PPh_3)_2(L)(bipy)]PF_6$, in which L represents the anionic ligand.

All the synthesized ruthenium complexes, *trans*-$[Ru(PPh_3)_2$(*N*,*N*-dibutyl-*N*′-benzoylthioureato-k^2O,S)(bipy)]PF_6 **(1)**, *trans*-$[Ru(PPh_3)_2$(*N*,*N*-dimethyl-*N*′-thiophenylthioureato-k^2O,S)(bipy)]PF_6 **(2)**, and *trans*-$[Ru(PPh_3)_2$(*N*,*N*-dimethyl-*N*′-benzoylthioureato-k^2O,S)(bipy)]PF_6 **(3)**, are of brown color and are electrolyte 1:1 in dichloromethane.

The data from the infrared spectra presented in the Material and methods suggest the formation of *trans*-$[Ru(PPh_3)_2$(acylthioureato-k^2O,S)(bipy)]PF_6 complexes **(1–3)**, where L is an anionic ligand, formed by the deprotonation of the *N*,*N*-disubstituted-*N*′-acylthiourea during its coordination to the ruthenium metal [35–39] (please see Supplementary information).

The electronic absorption spectra of **(1–3)** were recorded at room temperature using CH_2Cl_2 solvent, exhibiting three bands. The most intense absorption around 280 nm is assigned to the intraligand transition ($\pi \rightarrow \pi^*$) of the PPh_3, bipy and acylthiourea ligands, because similar absorptions are also observed for the free ligands. It is reasonable that this absorption is more intense in all the complexes because all the three ligands present conjugated π system. The less intense and lower-energy absorptions around 400 and 470 nm are assigned to the metal-to-ligand charge transfer (MLCT) $d\pi(Ru) \rightarrow \pi^*$ (ligand) transitions. The UV/Vis spectra of the complexes in the biological medium (DMEM + 0.1% DMSO), were also used to evaluate the stability of the complexes. Thus, after 48 h they were the same as those obtained in fresh solutions.

The X-ray structure of complex **(3)** is presented in Fig. 2, data collections and experimental details from crystal structure determination are summarized in Table S1 and the selected bond distances (Å) and angles (o) of complex **(3)** in Table S2. The single crystal XRD results demonstrated that complex **(3)** belonged to the monoclinic crystal

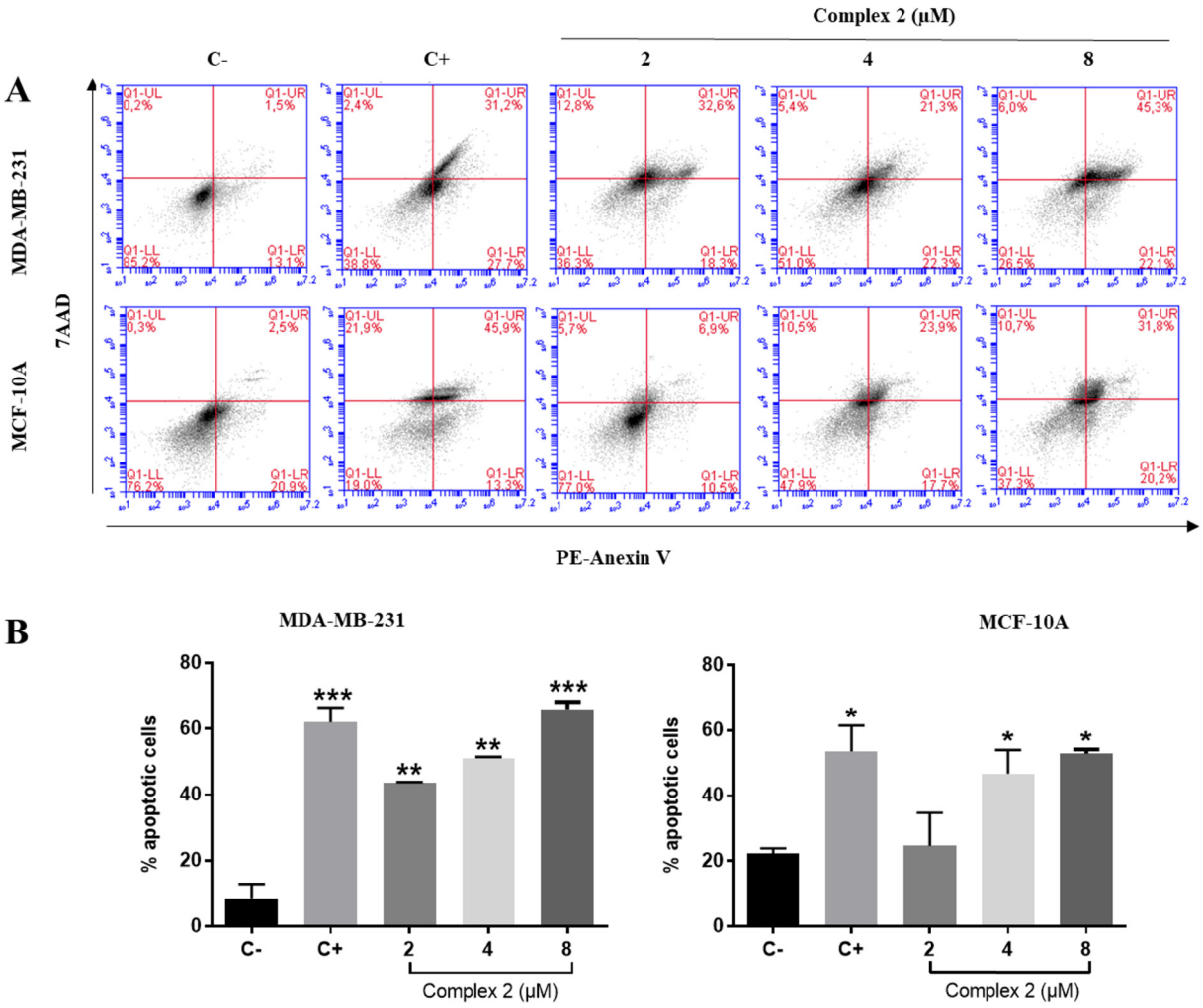

Fig. 6. Effects of complex **(2)** on apoptosis of MDA-MB-231 and MCF-10A cells. (A) Apoptosis assay with PE-Annexin V (detected in the FL2-A channel) and 7AAD (detected in the FL3-A channel) (B) Percentages of apoptosis induced by complex **(2)** on MDA-MB-231 and MCF-10A after 2 h of treatment with 2, 4 or 8 μM of the complex **(2)**. The experiments were performed in triplicate. Images correspond to one of triplicates. Camptothecin was used as a positive control (C+). Results were compared with negative control (C−) (untreated) (*$p \leq 0.05$, **$p \leq 0.01$).

system with space group $P2_1/a$. The X-ray structure of the complex **(3)** confirmed that the *N*,*N*-dimethyl-*N*′-benzoylthioureato anion is coordinated to the central ion Ru as bidentate ligand, by the oxygen and sulfur atoms, and there are two PPh_3 ligands, which are in the *trans* fashion, as also suggested by $^{31}P\{^1H\}$ NMR experiment as well (see below).

For the complex **(3)** the distance of C−S, 1.723(7) Å, is longer than the C−S bond distance of neutral species (1.661–1.676 Å), and the angles and distances found for the complex **(3)** are comparable to those found for other metalo-acylthiourea compounds [34,40–42]. The distance of C−O, 1.270(8) Å is a little longer than those found for typical C=O bonds, indicating its double-bond character, which is an evidence of resonance character in the ring formed by S−Ru−O, in the complex [34,40–42].

From the structural point of view complex **(1)** and **(2)** are similar to complex **(3)**, as shown in their $^{31}P\{^1H\}$ NMR spectra, where all of them present only a singlet, at about 27 ppm, as expected for the *trans* position of the triphenylphosphine ligands in the compounds. The NMR technique was also used to show the stability of the complexes in the biological medium. Thus, the $^{31}P\{^1H\}$ spectra of the complexes in the biological medium (DMEM + 0.1% DMSO), after 48 h was the same obtained in fresh solutions.

The redox behavior of complex **(1)** was investigated by cyclic voltammetry and differential pulse voltammetry (Fig. S1). The cyclic voltammogram of the complexes show a quasi-reversible process (Ia/Ip ~ 1) corresponding to a one-electron of the redox couple Ru^{III}/Ru^{II} (Table S3). The $E_{1/2}$ value found for the new complexes were considerably more anodic [(1), 853 mV; (2) 877 mV and (3) 753 mV], indicating better stabilization of the ruthenium center, when compared with the oxidation potential of the precursor *cis,trans*-$[RuCl_2(PPh_3)_2(bipy)]$ (E ½ = 420; Epa = 470 mV) [43]. It is worth to mention that in the range of 0 to 1.0 V, in the experimental condition here applied, the contra-ion PF_6^-, and the ligands triphenylphosphine, bipyridine and acylthioureas present no redox process in the cyclic voltammograms.

3.2. In vitro assays

The potential of ruthenium complexes acting on important steps of the metastatic process on breast cancer cell are already well described in the literature [44]. Therefore, the effects of the three *trans*-$[Ru(PPh_3)_2(acylthioureato\text{-}k^2O,S)(bipy)]PF_6$ complexes and the free ligands on TNBC MDA-MB-231 and non-tumor MCF-10A cells were further investigated (Table 1). For comparison, the cytotoxicity of cisplatin is also presented, since it is a successful anticancer drug that is still widely used in clinics [7]. Results demonstrate that complex **(2)** exhibited the highest SI, with the lowest IC_{50} for MDA-MB-231 cells (8.81 ± 0.81 μM) and the highest IC_{50} for MCF-10A

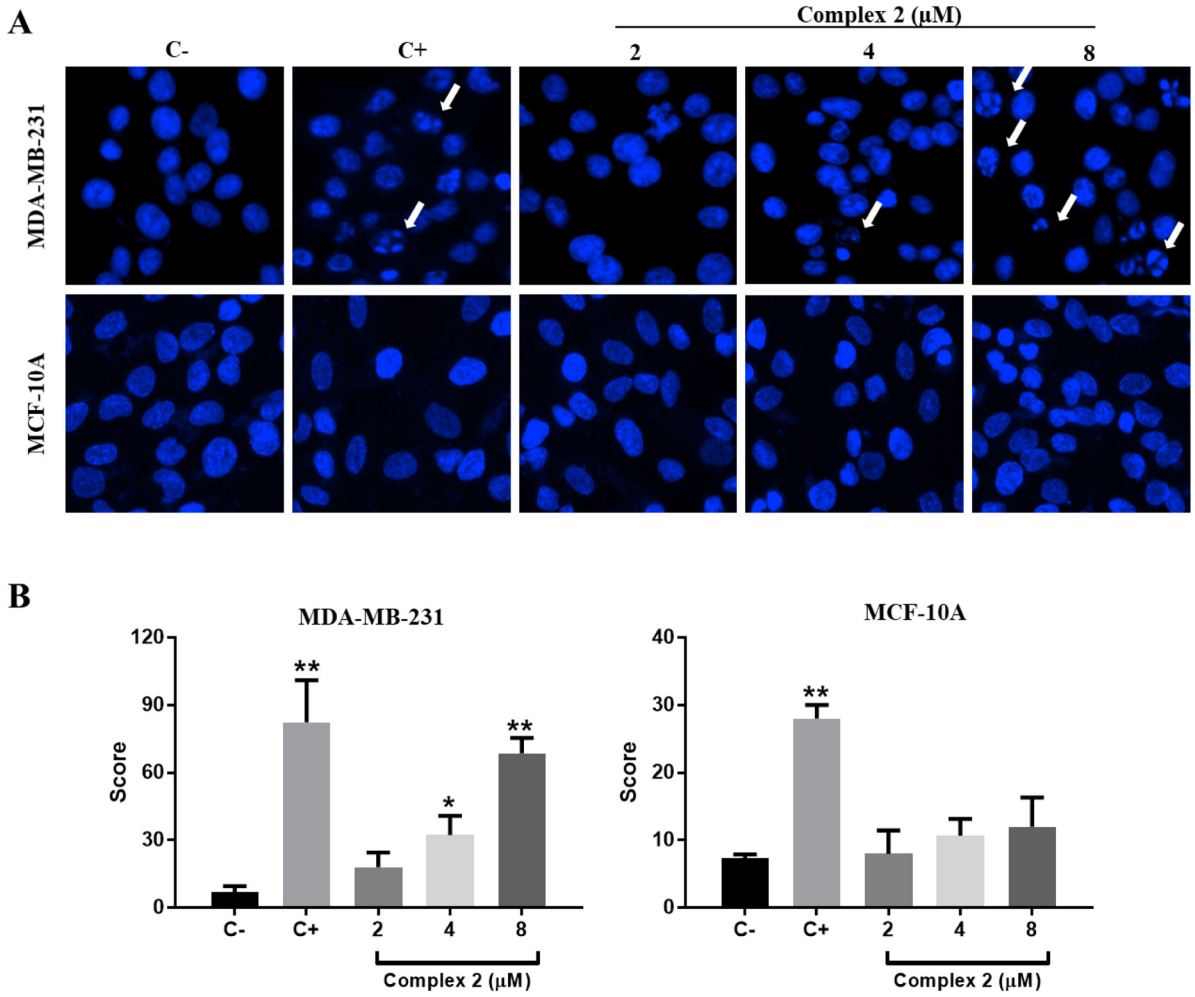

Fig. 7. Effects of complex **(2)** on DNA of MDA-MB-231 and MCF-10A cells. (A) Nuclear Fragmentation using DAPI staining after 2 h of treatment with 2, 4 or 8 μM of the complex **(2)**. Staurosporine was used as a positive control (C+). White arrows show fragmented nuclei. (B) Genotoxic effects of complex **(2)** on MDA-MB-231 and MCF-10A cells after 1 h of treatment with 2, 4 or 8 μM of the complex **(2)**. Cisplatin was used as a positive control (C+). The experiments were performed in triplicate. Images correspond to one of triplicates. Results were compared with negative control (C−) (untreated) (*$p \leq 0.05$, **$p \leq 0.01$).

(14.82 ± 2.50 μM) demonstrating to be the most effective among the three complexes tested. The results of this assay are in accordance with another work of the group where the smallest ligands were more active [45]. Thus, complex **(2)** was selected to be further investigated using *in vitro* and *in vivo* assays. In accordance with our results, another study using a ruthenium arene *o*-PDA complex, [(*p*-cym)Ru(*o*-pda)Cl]PF_6 (*o*-PDA), demonstrates that after 48 h of incubation the inhibition of the proliferation of MDA-MB-231 cells (83 μM) was more than three times higher than in MCF-10A cells (> 260 μM) showing that it also exhibits selectivity for tumor cells [46].

Different studies have shown that ruthenium complexes with similar structure to the complex **(2)** also have cytotoxic activity against different tumor cells. Four phosphinic ruthenium (II) complexes, *trans*-[$RuCl_2$(dppb)(dpqQX)], *cis*-[$RuCl_2$(dppb)(dpqQX)], *ct*-[RuCl(CO)(dppb)(dpqQX)]PF_6 and *ct*-[$RuCl_2(PPh_3)_2$(dpqQX)] were cytotoxic against MDA-MB-231 and MCF-7 cells, especially complex *ct*-[RuCl(CO)(dppb)(dpqQX)]PF_6, which demonstrated better activity compared to cisplatin [47]. Ruthenium(II)/triphenylphosphine complexes, *cis*-[Ru$(PPh_3)_2(lap)_2$] and trans-[Ru(lap)$(PPh_3)_2$(phen)]PF_6 were cytotoxic against MDA-MB-231, A549 (lung cancer) and V79 (non-tumor lung) cell lines, however the complex trans-[Ru(lap)$(PPh_3)_2$(phen)]PF_6 has lower IC_{50} than *cis*-[Ru$(PPh_3)_2(lap)_2$] and cisplatin [48]. Other nine ruthenium complexes with the general formula [Ru(AA-H)(dppb)(bipy)]PF_6 had their cytotoxic activity evaluated against the human MDA-MB-231 and DU-145 cells and also against a mouse cell line, Ehrlich. The results showed that almost all of the complexes tested were more active than cisplatin in the cell lines tested [49].

Morphological changes observed in MDA-MB-231 cells include decrease of cell density, formation of round-like structures and cell shrinkage, after 24 h of incubation, indicating an induction of cell death. On the other hand, complex **(2)** slightly altered MCF-10A cell morphology after 24 h at the highest concentration (12.5 μM) (Fig. 3A). In addition, in the clonogenic assay, complex **(2)** was able to completely inhibit the ability of MDA-MB-231 cells to form colonies at the highest concentration (2 μM) (Fig. 3B). There was also a significant decrease in the size and number of colonies at the lowest concentrations (0.5 and 1 μM). These results demonstrate that complex **(2)** has cytotoxic and cytostatic effects on TNBC cells.

The ability to migrate and invade circulation and other tissues is important to be studied by different methods because they represent key steps in the metastasis process *in vivo* [50]. The effect of complex **(2)** on MDA-MB-231 and MCF-10A cell migration was investigated using Boyden chambers and wound healing assays (Fig. 4A, B). The results of the Boyden chamber assay demonstrated that complex **(2)** was able to significantly inhibit the migration at all concentrations tested (1–4 μM) for both tumor and non-tumor cells (Fig. 4A). However, when comparing percentages of inhibition, it can be noted that complex **(2)** inhibits the migration of MDA-MB-231 cells more efficiently, with the concentration of 4 μM, inhibiting 90.8% of cell migration, while the percentage of inhibition was only 26.2% in the non-tumor cells. To

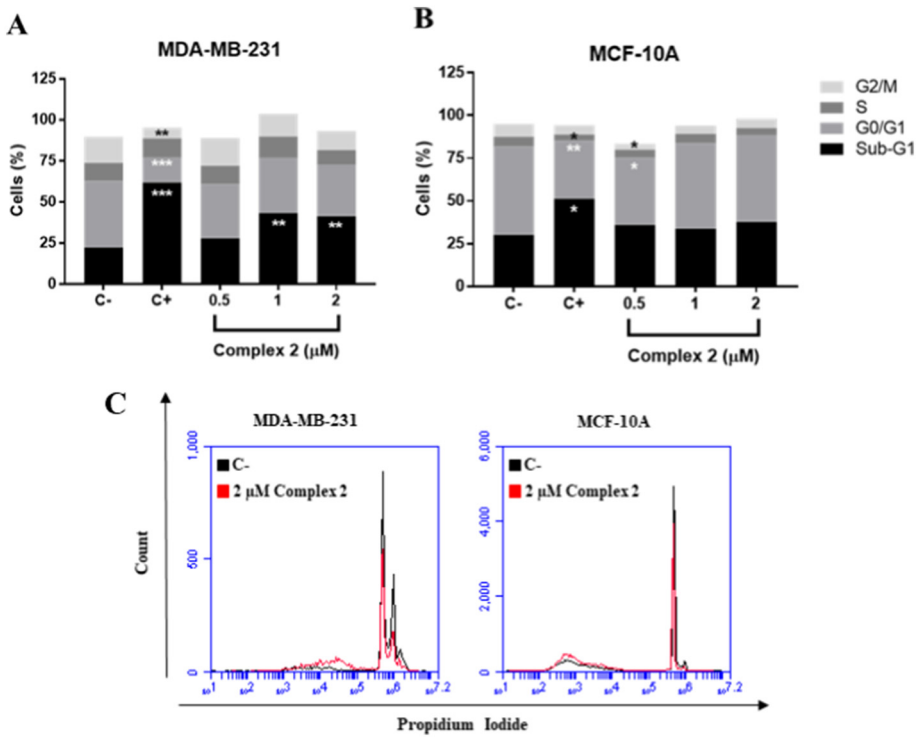

Fig. 8. Effects of complex **(2)** on cell cycle of MDA-MB-231 and MCF-10A cells. (A) Effects of complex **(2)** on cell cycle of MDA-MB-231 or (B) MCF-10A after 2 h of treatment with 0.5, 1 or 2 μM of the complex **(2)**. Camptothecin was used as a positive control (C+). (C) DNA histograms of the cell cycle assay with cells treated with propidium iodide (detected in the FL2-A channel). Untreated cells (negative control, C−) are shown in black and cells treated with 2 μM of the complex **(2)** for 2 h are shown in red. Camptothecin was used as a positive control (C+). The experiment was performed in triplicate. Results were compared with negative control (C−) (untreated) (*$p \leq 0.05$, **$p \leq 0.01$, ***$p \leq 0.001$).

further confirm this anti-migratory effect of complex **(2)** a wound healing assay was performed (Fig. 4B). The complex was more efficient to inhibit the migration of MDA-MB-231 compared to the migration of MCF-10A cells (yellow squares) after 24 h of incubation. In addition, complex **(2)** was able to significantly inhibit the invasion of both cells, MDA-MB-231 and MCF-10A, at all concentrations tested (1–4 μM) (Fig. 4C). However, once again it was more specific for tumor cells (79% inhibition), compared to non-tumor cells (61%).

It is important to point out that the incubation of complex **(2)** at 4 μM for 24 h can cause some cell death rather than impair migration and invasion of tumor cells. However, complex **(2)** was able to significantly inhibit tumor cell migration and invasion at lower concentrations (1 and 2 μM), which are not cytotoxic. This surely indicates that complex **(2)** is impairing migration and invasion processes in tumor cells, rather than being cytotoxic in these assays.

The interactions among extracellular matrix (ECM) proteins, adhesion receptors and the actin cytoskeleton are related to cell adhesion and are important in the regulation of several cell processes, such as growth, differentiation, shape and survival [51]. Complex **(2)** significantly inhibited MDA-MB-231 cell adhesion to different ECM components, such as collagen type I, fibronectin, laminin and vitronectin at all concentrations tested (2, 4 or 8 μM) (Fig. 5A). A phalloidin assay was performed in order to analyze the effect of different concentrations (2, 4, 8 or 16 μM) of complex **(2)** on cytoskeleton of MDA-MB-231 cells. Complex **(2)** induced changes in the actin cytoskeleton with subsequent loss of stress fibers formation in a concentration-dependent manner (Fig. 5B). Another work of our group demonstrated that a biphosphine/bipyridine ruthenium complex, $[Ru(CH_3CO_2)(dppb)(bipy)]PF_6$, was also able to inhibit adhesion, migration and invasion and to induce changes in the actin cytoskeleton in the TNBC MDA-MB-231 cells [22].

Induction of cell apoptosis has been suggested as a promising strategy for the development of anticancer drugs [52]. Complex **(2)** was able to induce apoptosis of both, MDA-MB-231 and MCF-10A cells, in a concentration-dependent manner (Fig. 6). At the lowest concentration (2 μM) the complex significantly induced apoptosis in 43% of the tumor cells, whereas in non-tumor cells the apoptosis rate was only approximately 24%. DAPI staining corroborates these results showing that complex **(2)** (2, 4 and 8 μM) more specific to tumor cells because it provoked nuclear chromatin condensation with formation of apoptotic bodies only in tumor cells (Fig. 7A).

The complex **(2)** was able to induce significant DNA damage in MDA-MB-231 cells at the concentrations of 4 and 8 μM, as well as the positive control, cisplatin (8 μM), as demonstrated by the comet assay. However, the complex did not cause significant DNA damage in MCF-10A cells, only cisplatin induced damage to these cells (Fig. 6B). Recently, other researchers have demonstrated that ruthenium complexes can induce DNA damage in different tumor cell lines. Polypyridyl ruthenium complexes, $[Ru(dmb)_2(DQTT)](ClO_4)_2$; $[Ru(bpy)_2(DQTT)](ClO_4)_2$; and $[Ru(dmp)_2(DQTT)](ClO_4)_2$, at 6.25 μM with a 24 h of incubation, were able to induce DNA fragmentation of BEL-7402 liver tumor cells [53]. Others ruthenium polypyridyl complexes, $[Ru(bpy)_2(FTTP)](ClO_4)_2$; $[Ru(phen)_2(FTTP)](ClO_4)_2$; $[Ru(bpy)_2(PTTP)](ClO_4)_2$ and $[Ru(phen)_2(PTTP)](ClO4)_2$, were also able to induce DNA damage of HepG2 liver tumor cells after 24 h of incubation with 12.5 μM [54].

In order to investigate whether complex **(2)** would interfere on MDA-MB-231 and MCF-10A cell cycle, an assay using PI staining of DNA content was performed. In MDA-MB-231 cells, complex **(2)** significantly arrested cell cycle at sub-G1 phase at the highest concentrations, indicating DNA fragmentation (Fig. 8A). In MCF-10A cells, complex **(2)** only significantly reduced the quantity of DNA at G0/G1 and G2/M at the lowest concentration (Fig. 8B). These results show that complex **(2)** induced apoptosis in MDA-MB-231 cells also by preventing cells from entering the cell cycle. In agreement with our study, another work verified that two different ruthenium complexes containing acylthiourea ligands also are able to induce cell cycle arrest at sub-G1 phase and apoptosis cell death of the MDA-MB-231 cells [40].

Since complex **(2)** presented a pro-apoptotic effect, especially in the tumor cells, a further investigation of its action on the expression of apoptosis-related genes such as Bax, caspase-3 and Bcl-2, as well as in protein level of apoptosis-related molecules, Bax, caspase-3 and Bcl-2 was explored (Fig. 9). The effects of complex **(2)** on anti- and pro-apoptotic genes were investigated by real time quantitative PCR (qRT-PCR, Fig. 9A). In tumor cells, complex **(2)** significantly increased the

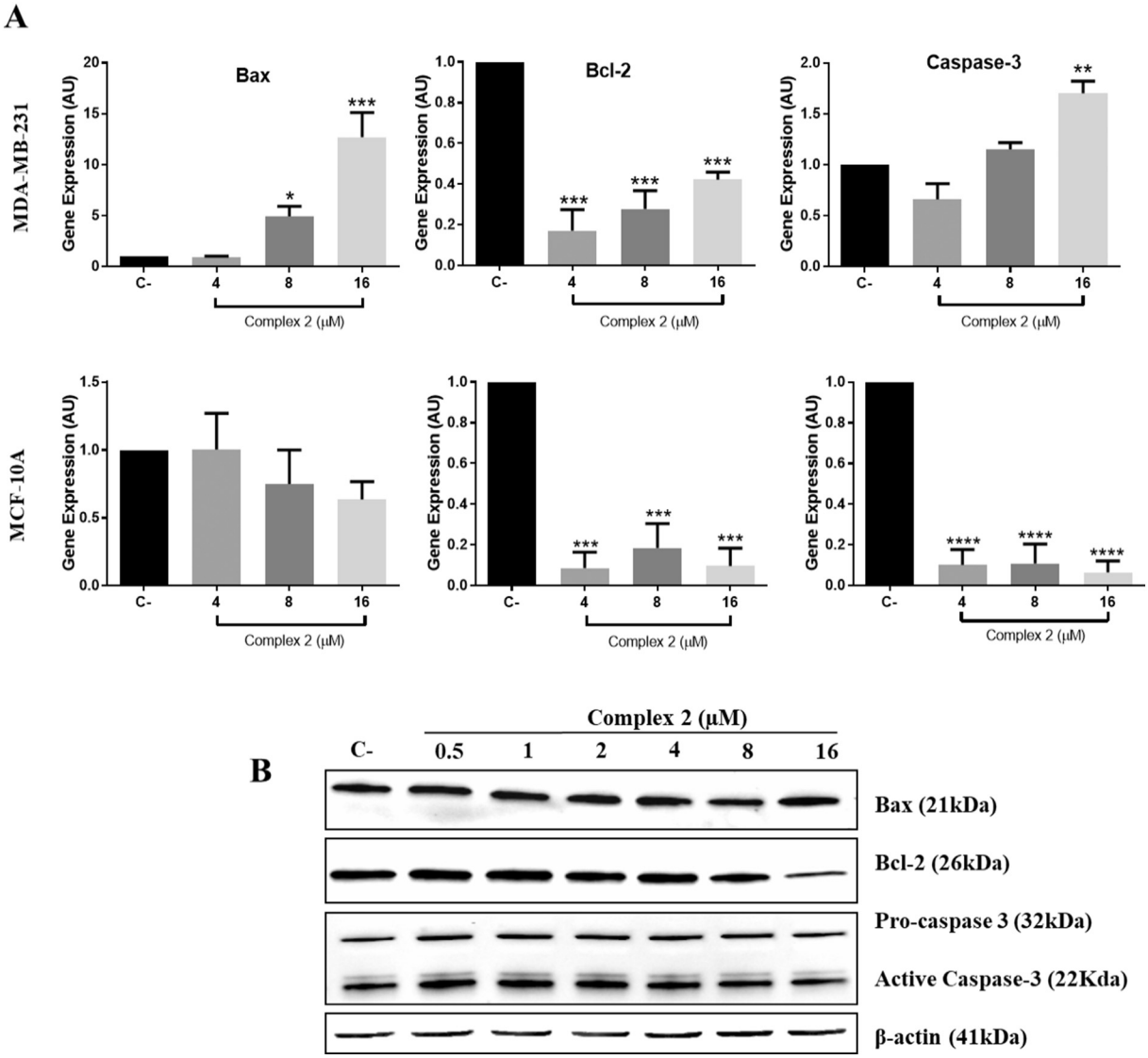

Fig. 9. Effects of complex **(2)** on expression and on the protein content of apoptotic and anti-apoptotic molecules of MDA-MB-231 and MCF-10A cells. (A) qRT-PCR after 2 h of treatment with the indicated concentrations of the complex **(2)** and (B) Western blotting analysis after 4 h of treatment with the indicated concentrations of the complex **(2)**. The experiments were performed in triplicate. Results were compared with negative control (C−) (untreated) (*$p \leq 0.05$, **$p \leq 0.01$, ***$p \leq 0.001$).

expression of Bax and caspase-3 and significantly decreased the expression of Bcl-2. In MCF-10A cells, complex **(2)** did not alter Bax gene expression, significantly decreased Bcl-2 and caspase-3 gene expression at all concentrations tested (4, 8 and 16 μM). These results are in accordance with our previous apoptosis-related assays and demonstrate that in MCF-10A cells the caspase-3 encoding gene, which is the key performer of the apoptosis process, is not increased and may explain nuclear integrity in this cell line.

Then, the expression of Bax, Bcl-2 and caspase-3 in MDA-MB-231 cells was investigated (Fig. 9B). After 4 h treatment with complex **(2)**, the expression of Bax increased, whereas the reverse occurs with Bcl-2 in the highest concentration (16 μM). These results support the data of qRT-PCR demonstrating that Bax levels are increased and Bcl-2 levels are down regulated after incubation with complex **(2)**. However, caspase-3 protein levels did not alter, while its gene expression is increased in all concentrations tested, probably due to shorter incubation times used in the gene expression assays compared to Western blotting assays.

Ruthenium(II) complexes with a chloro-substituted phenylazopyridine ligand, $[Ru(Clazpy)_2bpy]Cl_2{\cdot}7H_2O$ and $[Ru(Clazpy)_2phen]Cl_2{\cdot}8H_2O$, are also able to induce apoptosis and to inhibit cell cycle through the upregulation of genes related to these events after 24 h treatment in MDA-MB-231, BRCA1-defective HCC1937 and BRCA1-competent MCF-7 cells. Interestingly complex $[Ru(Clazpy)_2phen]Cl_2{\cdot}8H_2O$ can also downregulate in the HCC1937 cells the mRNA of the breast cancer susceptibility gene 1 (BRCA1) [55], which is commonly mutated in TNBC cells. These data suggest that ruthenium complexes can be an alternative to treat triple negative cancers [56].

3.3. *In vivo* assays

In the *in vivo* acute toxicity test doses were administered over a 24 h period and animals observed for 14 days to identify possible signs of toxicity and related deaths [32]. The acute toxicity assay revealed that with the initial dose (50 mg/kg) administrated intraperitoneally to 3 animals, no deaths occurred on the first 24 h. This procedure was repeated, and results were identical. Then, this procedure was repeated twice with a higher dose (300 mg/kg) with no deaths. After each treatment, the animal's behavior was observed for the period of 14 days in the search for signs that could identify toxicity. There were no

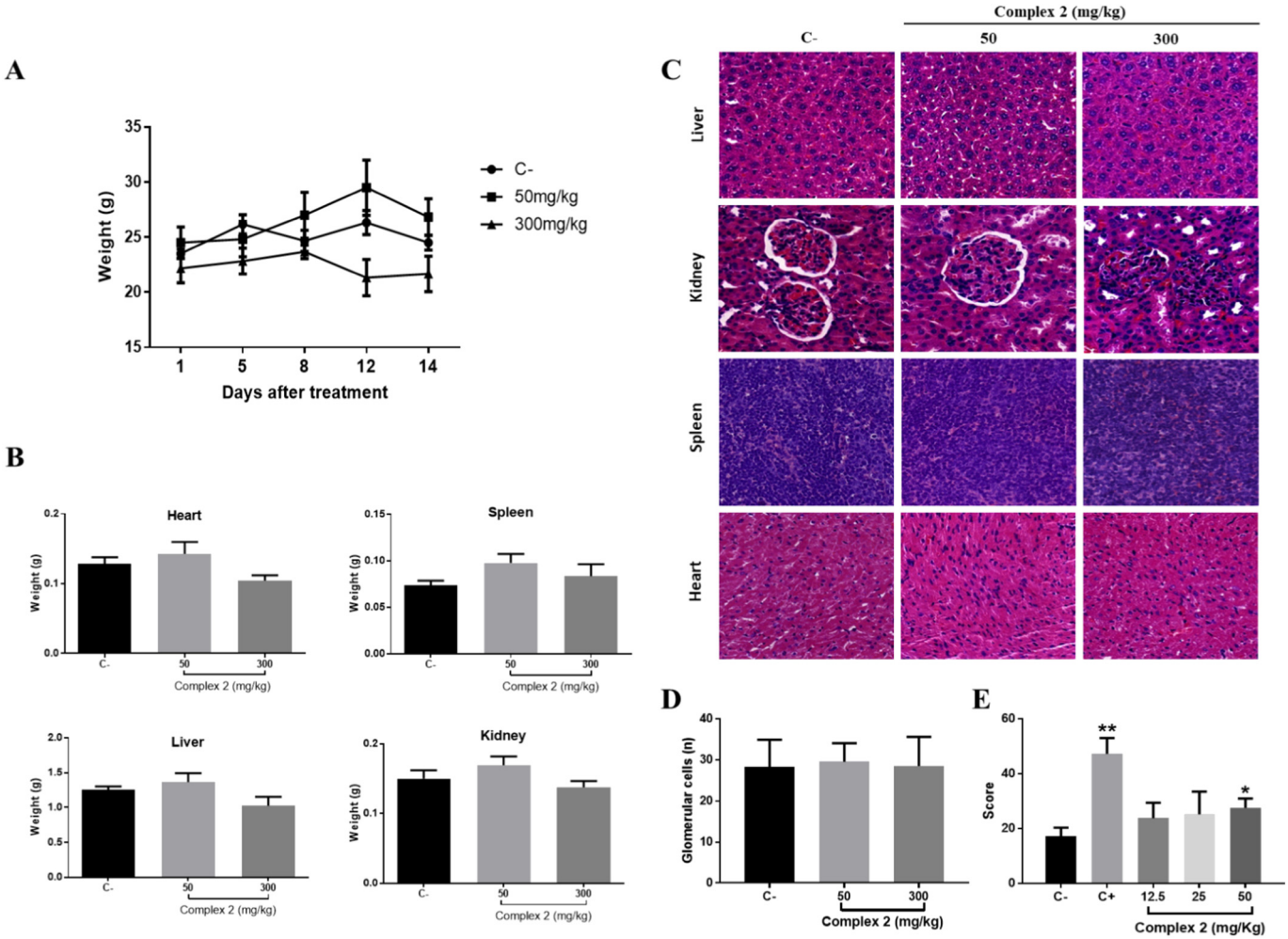

Fig. 10. Effects of complex **(2)** *in vivo* after the treatment with 50 or 300 mg/kg of the complex **(2)**. (A) Weight of animals over a period of 14 days, (B) weight of animal's organs after euthanasia, (C) histological analysis of animal's organs with HE, (D) glomerular analysis and (E) *in vivo* comet assay. Results were compared with negative control (C−) (untreated) (*$p \leq 0.05$, **$p \leq 0.01$, ***$p \leq 0.01$).

behavioral or skin, pelage, eyes and membranes changes. Animals exhibited a normal behavior, characteristic of the species. The animal's weight was also monitored from the beginning of treatment until day 14. Complex **(2)** at the doses administered intraperitoneally (50 and 300 mg/kg) was not able to significantly alter the animals' (Fig. 10A) or organs' weight (Fig. 10B), compared to the control groups, indicating no signals of toxicity. Accordingly, histopathological analysis showed no signs of inflammation or degeneration in the kidneys (Fig. 10C). However, at the highest dose (300 mg/kg), the decrease in Bowman's space of the glomeruli was perceived. To verify whether there was an alteration in glomerular cell proliferation, 40 glomeruli in each group were counted in random fields, however, no significant changes in the number of these cells (Fig. 10D) was found. Additionally, no morphological or pathological alterations were found in the spleens, livers and hearts analyzed, demonstrating that complex **(2)** did not cause organ toxicity.

Other studies also evaluated the *in vivo* toxicity of ruthenium complexes. Grozav et al. [57] evaluated the toxicity of the ruthenium complex, [(η^6-*p*-cymene)Ru(L)Cl]Cl (L = 1-(2-(2-(3-chlorobenzylidene) hydrazinyl)-4-methylthiazol-5-yl)ethanone), *in vivo* in *Wistar* rat females. Doses (50, 300 and 2000 mg/kg) were administered orally in one group and intraperitoneally in another group and the animals were observed for 14 days. The results showed that the complex orally administrated presented median lethal dose (LD_{50}) higher than 2000 mg/kg and that there were no behavioral, hematological, histopathological and weight changes in the animals during the observation period. The results showed no hematological and weight changes, but the LD_{50} value was between 300 and 2000 mg/kg and there where moderate lymphocytosis in the spleen in the group that received the dose of 2000 mg/kg. In another study, six ruthenium complexes [Ru(pic)(dppb)(bipy)]PF_6 (SCAR1), [Ru(pic)(dppb)(Me-bipy)]PF_6 (SCAR2), [Ru(pic)(dppb)(phen)]PF_6 (SCAR4), *cis*-[Ru(pic)(dppe)2]PF_6 (SCAR5), *cis*-[$RuCl_2$(dppb)(bipy)] (SCAR6) and [Ru(pic)(dppe)(phen)]PF_6 (SCAR7), were evaluated for acute oral toxicity in female C57BL/6 mice. The initial concentration used was 2000 mg/kg and when it caused death in > 50% of the group of 6 animals a lower dose was administered. The results showed that only SCAR1, SCAR4 and SCAR6 have low toxicity at the doses tested (2000, 1000 and 500 mg/kg) [58].

The results of genotoxic evaluation of complex **(2)** indicated that only the group of animals treated with the highest dose (50 mg/kg) and the animals treated with positive control, doxorubicin, presented DNA damage (Fig. 10E). Doxorubicin is commonly used as a positive control for comet assays because it is recognized for causing DNA damaging [59–61]. It is important to highlight that although significant DNA damage has been observed in the highest dose, the DNA damage in the cells (nucleoids) was predominantly minor (class 1 - data not shown), with only a few cells showing a large amount of damage (classes 2 and 3).

In the literature there are already interesting results regarding the use of ruthenium complexes for the treatment of triple negative breast

tumors *in vivo*. The effects of an organometallic ruthenium (II) [(η^6-*p*-Cymene)Ru{(Ph_3P═N−CO-2-N-C_5H_4)-κ-N,O}Cl]Cl on MDA-MB-231 xenografts in female NOD.CB17-Prkdc SCID/J mice was evaluated after 28 days of treatment with a total of 14 doses of 5 mg/kg administered every other day. The results demonstrated that the ruthenium complex was able to inhibit and reduce the tumors and further studies demonstrated also that this complex presents low systemic toxicity [62]. Another study demonstrated that another organometallic ruthenium (II) complex [Ru(*p*-cymene)(bis(3,5-dimethylpyrazol-1-yl)methane)Cl]Cl, denominated UNICAM-1, can also reduce significantly, with low toxicity, the growth of the triple negative tumor in female FVB/NCrl mice in an experimental TNBC model, which doses of 52 mg/kg/day repeated 4 times at intervals of 3 days were administrated [63]. Through these studies it is possible to conclude that ruthenium complexes are good candidates for further evaluation as a potential drug for triple negative breast tumors and these results encourages new studies with complex **(2)** *in vivo*.

4. Conclusions

Three *trans*-[$Ru(PPh_3)_2$(acylthioureato-k^2O,S)(bipy)]PF_6 complexes were synthesized, characterized and their cytotoxicity activity were evaluated in MDA-MB-231 tumor cells and in the non-tumor MCF-10A cells. The *trans*-[$Ru(PPh_3)_2$(*N*,*N*-dimethyl-*N*′-thiophenylthioureato-k^2O,S)(bipy)]PF_6, complex **(2)**, was found to be the most active against TNBC MDA-MB-231 tumor cells, among the three complexes. Complex **(2)** inhibited proliferation, migration, invasion, adhesion, changed morphology and induced apoptosis, DNA damage and nuclear fragmentation of TNBC cells at lower concentrations compared to non-tumor MCF-10A cells, suggesting an effective action for this complex on tumor cells. Finally, complex **(2)** *in vivo* did not induce toxicity and caused DNA damage only at the highest dose administrated. Our results indicate that complex **(2)** has potential in cancer therapy based on its antiproliferative and apoptosis inducing effects *in vitro* and also on its low toxicity and genotoxic properties *in vivo*. More studies need to be performed in order to demonstrate its *in vivo* effects on cancer treatment, using animal models.

Supplementary data to this article can be found online at https://doi.org/10.1016/j.jinorgbio.2018.05.011.

Abbreviations

7AAD	7-aminoactinomycin D
BRCA1	breast cancer susceptibility gene 1
Bipy	2,2′-bipyridine
BSA	bovine serum albumine
CH_2Cl_2	methylene chloride
CsI	cesium iodide
DAPI	4′,6-diamidino-2-phenylindole
DMEM	Dulbecco's Modified Eagle's Medium
DMSO	dimethyl sulfoxide
EDTA	ethylenediamine tetraacetic acid
FBS	fetal bovine serum
HE	hematoxylin and eosin
HER-2	human epidermal growth factor 2
IC_{50}	half-maximal inhibitory concentration
IR	infrared region
MTT	[3-(4,5-dimethylthiozol-2-yl)-2,5-diphenyltetrazolium bromide]
MLCT	metal-to-ligand charge transfer
PE-annexin-V	phycoerythrin-annexin V
PI	propidium iodide
qRT-PCR	real time quantitative polymerase chain reaction
RNase	ribonuclease
TBAP	Bu_4NClO_4
TNBC	triple negative breast cancer

Conflict of interest

The authors declare that they have no conflict of interest.

Acknowledgements

The authors are grateful for the financial support of FAPESP (São Paulo Research Foundation, grants #2013/00798-2 and #2015/24940-8), to Dr. Edson Garcia Soares for his supervision in the analysis of the histology slides, to Dr. Angelina Maria Fuzer to her assistance in the design of the graphical abstract and to Larissa Zochio de Souza for her technical assistance in the *in vivo* comet assay. A. B. Becceneri has a scholarship sponsored by FAPESP, grant #2014/25121-8.

Author contributions

Study design: A.B.B., A.A.B. and M.R.C.; Experimental work: A.B.B., C.P.P., A.M.P., E.L.M. and E.E.C.; Data analysis and interpretation: All authors; Manuscript preparation: A.B.B., A. M. P., A.A.B. and M.R.C.; Manuscript editing: A.B.B., A.A.B. and M.R.C. Manuscript review: All authors.

Notes

Crystallographic data have been deposited with the deposition code CCDC 1589058 for complex 3. Copy of this information may be obtained from the Director, Cambridge Crystallographic Data Centre (CCDC), 12 Union Road, Cambridge CB2 1EZ, UK, Fax: +44 1233 336,033, E-mail: deposit@ccdc.cam.ac.uk or http://www.ccdc.cam.ac.uk/conts/retrieving.html.

References

[1] V.G. Abramson, B.D. Lehmann, T.J. Ballinger, J.A. Pietenpol, Cancer 121 (2015) 8–16.
[2] J. Collignon, L. Lousberg, H. Schroeder, G. Jerusalem, Breast Cancer (Dove Med Press) 8 (2016) 93–107.
[3] H.A. Wahba, H.A. El-Hadaad, Cancer Biol. Med. 12 (2015) 106–116.
[4] P.C. Bruijnincx, P.J. Sadler, Curr. Opin. Chem. Biol. 12 (2008) 197–206.
[5] X. Kang, H.H. Xiao, H.Q. Song, X.B. Jing, L.S. Yan, R.G. Qi, Cancer Biol. Med. 12 (2015) 362–374.
[6] N.J. Wheate, S. Walker, G.E. Craig, R. Oun, Dalton Trans. 39 (2010) 8113–8127.
[7] L. Kelland, Nat. Rev. Cancer 7 (2007) 573–584.
[8] I. Kostova, Recent Pat. Anticancer Drug Discov. 1 (2006) 1–22.
[9] M. Abid, F. Shamsi, A. Azam, Mini Rev. Med. Chem. 16 (2016) 772–786.
[10] M.J. Clarke, Coord. Chem. Rev. 232 (2002) 69–93.
[11] C.S. Allardyce, P.J. Dyson, Platin. Met. Rev. 45 (2001) 62–69.
[12] W. Hernández, E. Spodine, J.C. Muñoz, L. Beyer, U. Schröder, J. Ferreira, M. Pavani, Bioinorg. Chem. Appl. 1 (2003) 271–284.
[13] A.M. Plutin, H. Marquez, E. Ochoa, M. Morales, M. Sosa, L. Moran, Y. Rodriguez, M. Suarez, N. Martin, C. Seoane, Tetrahedron 56 (2000) 1533–1539.
[14] M. Mureseanu, A. Reiss, N. Cioatera, I. Trandafir, V. Hulea, J. Hazard. Mater. 182 (2010) 197–203.
[15] R.R. Cairo, A.M.P. Stevens, T.D. de Oliveira, A.A. Batista, E.E. Castellano, J. Duque, D.B. Soria, A.C. Fantoni, R.S. Correa, M.F. Erben, Spectrochim. Acta A 176 (2017) 8–17.
[16] Enraf-Nonius, Collect, Nonius BV, Delft, The Netherlands, 1997–2000.
[17] Z. Otwinowski, W. Minor, Method Enzymol. 276 (1997) 307–326.
[18] R.H. Blessing, Acta Crystallogr. A. 51 (1995) 33–38.
[19] G.M. Sheldrick, ShelXS-97 Program for Crystal Structure Resolution, University of Göttingen, Göttingen, Germany, 1997.
[20] L.J. Farrugia, J. Appl. Crystallogr. 30 (1997) 565–566.
[21] T. Mosmann, J. Immunol. Methods 65 (1983) 55–63.
[22] C.P. Popolin, J.P.B. Reis, A.B. Becceneri, A.E. Graminha, M.A.P. Almeida, R.S. Correa, L.A. Colina-Vegas, J. Ellena, A.A. Batista, M.R. Cominetti, PLoS One 12 (2017) e0183275.
[23] J.C. Filho, A.L. Sarria, A.B. Becceneri, A.M. Fuzer, J.R. Batalhao, C.M. da Silva, R.M. Carlos, P.C. Vieira, J.B. Fernandes, M.R. Cominetti, PLoS One 9 (2014) e107058.
[24] A.M. Fuzer, J.C. Filho, A.B. Becceneri, D.A. Dos Santos, M.F. da Silva, P.C. Vieira, J.B. Fernandes, H.S. Selistre-de-Araujo, C.M. Cazal, M.R. Cominetti, Anticancer agents, Med. Chem. 13 (2013) 1645–1653.
[25] C.W. Zeng, X.J. Zhang, K.Y. Lin, H. Ye, S.Y. Feng, H. Zhang, Y.Q. Chen, Mol. Pharmacol. 81 (2012) 578–586.
[26] C.A. Belmokhtar, J. Hillion, E. Segal-Bendirdjian, Oncogene 20 (2001) 3354–3362.

[27] A.C.B.M. Martin, A.M. Fuzer, A.B. Becceneri, J.A. da Silva, R. Tomasin, D. Denoyer, S.H. Kim, K.A. McIntyre, H.B. Pearson, B. Yeo, A. Nagpal, X. Ling, H.S. Selistre-de-Araujo, P.C. Vieira, M.R. Cominetti, N. Pouliot, Oncotarget 8 (2017) 72260–72271.
[28] K.J. Livak, T.D. Schmittgen, Methods 25 (2001) 402–408.
[29] R.R. Tice, E. Agurell, D. Anderson, B. Burlinson, A. Hartmann, H. Kobayashi, Y. Miyamae, E. Rojas, J.C. Ryu, Y.F. Sasaki, Environ. Mol. Mutagen. 35 (2000) 206–221.
[30] A. Azqueta, S. Meier, C. Priestley, K.B. Gutzkow, G. Brunborg, J. Sallette, F. Soussaline, A. Collins, Mutagenesis 26 (2011) 393–399.
[31] A. Hartmann, G. Speit, Toxicol. Lett. 90 (1997) 183–188.
[32] Organisation for Economic Cooperation and Development (OECD), Test No. 423: Acute Oral toxicity - Acute Toxic Class Method, OECD Guidelines for the Testing of Chemicals, Section 4, No. 423, OECD Publishing, Paris, 2001. https://doi.org/10.1787/9789264071001-en , Accessed date: 15 January 2018.
[33] Organisation for Economic Cooperation and Development (OECD), Test No. 489: In Vivo Mammalian Alkaline Comet Assay, OECD Guidelines for the Testing of Chemicals, Section 4, No. 489, OECD Publishing, Paris, 2016. https://doi.org/10.1787/9789264264885-en , Accessed date: 20 January 2018.
[34] R.S. Correa, K.M. de Oliveira, F.G. Delolo, A. Alvarez, R. Mocelo, A.M. Plutin, M.R. Cominetti, E.E. Castellano, A.A. Batista, J. Inorg. Biochem. 150 (2015) 63–71.
[35] A.E. Graminha, C. Rodrigues, A.A. Batista, L.R. Teixeira, E.S. Fagundes, H. Beraldo, Spectrochim. Acta A Mol. Biomol. Spectrosc. 69 (2008) 1073–1076.
[36] P.I.D.S. Maia, A.E. Graminha, F.R. Pavan, C.Q.F. Leite, A.A. Batista, D.F. Back, E.S. Lang, J. Ellena, S.d.S. Lemos, H.S. Salistre-de-Araujo, V.M. Deflon, J. Braz. Chem. Soc. 21 (2010) 1177–1186.
[37] A.P. Rebolledo, L.R. Teixeira, A.A. Batista, A.S. Mangrich, G. Aguirre, H. Cerecetto, M. Gonzalez, P. Hernandez, A.M. Ferreira, N.L. Speziali, H. Beraldo, Eur. J. Med. Chem. 43 (2008) 939–948.
[38] A.P. Rebolledo, M. Vieites, D. Gambino, O.E. Piro, E.E. Castellano, C.L. Zani, E.M. Souza-Fagundes, L.R. Teixeira, A.A. Batista, H. Beraldo, J. Inorg. Biochem. 99 (2005) 698–706.
[39] K. Nakamato, Infrared and Raman Spectra of Inorganic and Coordination Compounds, 5 ed., Wiley-Interscience, New York, 1997.
[40] L. Colina-Vegas, L. Luna-Dulcey, A.M. Plutin, E.E. Castellano, M.R. Cominetti, A.A. Batista, Dalton Trans. 46 (2017) 12865–12875.
[41] R.S. Correa, K.M. Oliveira, H. Pérez, A.M. Ana, M. Plutin, R. Ramos, R. Mocelo, E.E. Castellano, A.A. Batista, Arab. J. Chem. 150 (2015).
[42] J.P. Barolli, P.I.S. Maia, L. Colina-Vegas, J. Moreira, A.M. Plutin, R. Mocelo, V.M. Deflon, M.R. Cominetti, M.I. Camargo-Mathias, A.A. Batista, Polyhedron 126 (2017) 33–41.
[43] A.A. Batista, M.O. Santiago, C.L. Donnici, I.S. Moreira, P.C. Healy, S.J. Berners-Price, S.L. Queiroz, Polyhedron 20 (2001) 2123–2128.
[44] C.P. Popolin, M.R. Cominetti, Mini. Rev. Med. Chem. 17 (2017) 1435–1441.
[45] A.M. Plutin, A. Alvarez, R. Mocelo, R. Ramos, E.E. Castellano, M.M. Silva, W. Villarreal, F.R. Pavan, C.S. Meira, J.S. Rodrigues Filho, D.R.M. Moreira, M.B.P. Soares, A.A. Batista, Polyhedron 132 (2017) 70–77.
[46] J. Iida, E.T. Bell-Loncella, M.L. Purazo, Y. Lu, J. Dorchak, R. Clancy, J. Slavik, M.L. Cutler, C.D. Shriver, J. Transl. Med. 14 (2016).
[47] J.P. Barolli, R.S. Correa, F.S. Miranda, J.U. Ribeiro, C. Bloch Jr., J. Ellena, V. Moreno, M.R. Cominetti, A.A. Batista, J. Braz. Chem. Soc. 28 (2017) 1879–1889.
[48] K.M. Oliveira, R.S. Correa, M.I.F. Barbosa, J. Ellena, M.R. Cominetti, A.A. Batista, Polyhedron 130 (2017) 108–114.
[49] A.P. Almeida, F.B. Nascimento, A.E. Graminha, A.G. Ferreira, J. Ellena, F.M.S. Mello, A.P. Lima, E.P. Silveira-Lacerda, A.A. Batista, Polyhedron 81 (2014) 735–742.
[50] C.R. Justus, N. Leffler, M. Ruiz-Echevarria, L.V. Yang, J. Vis. Exp. 88 (2014).
[51] G. Pawlak, D.M. Helfman, Curr. Opin. Genet. Dev. 11 (2001) 41–47.
[52] G. Pistritto, D. Trisciuoglio, C. Ceci, A. Garufi, G. D'Orazi, Aging 8 (2016) 613–619.
[53] C. Zhang, B.J. Han, C.C. Zeng, S.H. Lai, W. Li, B. Tang, D. Wan, G.B. Jiang, Y.J. Liu, J. Inorg. Biochem. 157 (2016) 62–72.
[54] D. Wan, S.H. Lai, H.H. Yang, B. Tang, C. Zhang, H. Yin, C.C. Zeng, Y.J. Liu, J. Photochem. Photobiol. B 165 (2016) 246–255.
[55] T. Nhukeaw, P. Temboot, K. Hansongnern, A. Ratanaphan, BMC Cancer 14 (2014).
[56] K. Hongthong, A. Ratanaphan, Curr. Cancer Drug Targets 16 (2016) 606–617.
[57] A. Grozav, V. Miclaus, O. Vostinaru, S. Ghibu, C. Berce, I. Rotar, C. Mogosan, B. Therrien, F. Loghin, D.S. Popa, Regul. Toxicol. Pharmacol. 80 (2016) 233–240.
[58] F.R. Pavan, G.V. Poelhsitz, L.V. da Cunha, M.I. Barbosa, S.R. Leite, A.A. Batista, S.H. Cho, S.G. Franzblau, M.S. de Camargo, F.A. Resende, E.A. Varanda, C.Q. Leite, PLoS One 8 (2013) e64242.
[59] E.S. Marques, D.B. Salles, E.L. Maistro, Toxicol. Rep. 2 (2015) 268–274.
[60] P.M. Terrazas, E. de Souza Marques, L.N. Mariano, V. Cechinel-Filho, R. Niero, S.F. Andrade, E.L. Maistro, PLoS One 8 (2013) e76485.
[61] D.D. Leffa, B.N. Bristot, A.P. Damiani, G.D. Borges, F. Daumann, G.M. Zambon, G.E. Fagundes, V.M. de Andrade, Mol. Neurobiol. 53 (2016) 5575–5581.
[62] M. Frik, A. Martinez, B.T. Elie, O. Gonzalo, D. Ramirez de Mingo, M. Sanau, R. Sanchez-Delgado, T. Sadhukha, S. Prabha, J.W. Ramos, I. Marzo, M. Contel, J. Med. Chem. 57 (2014) 9995–10012.
[63] M. Montani, G.V.B. Pazmay, A. Hysi, G. Lupidi, R. Pettinari, V. Gambini, M. Tilio, F. Marchetti, C. Pettinari, S. Ferraro, M. Iezzi, C. Marchini, A. Amici, Pharmacol. Res. 107 (2016) 282–290.